https://ntrs.nasa.gov/search.jsp?R=19620004070 2020-03-11T13:21:43+00:00Z

CASE FILE COPY

N 62 14070

NASA TN D-1368

NASA TN D-1368

TECHNICAL NOTE

D-1368

STUDY OF UMBRELLA-TYPE ERECTABLE PARABOLOIDAL SOLAR CONCENTRATORS FOR GENERATION OF SPACECRAFT AUXILIARY POWER

By William D. Nowlin and Harold E. Benson

Langley Research Center
Langley Station, Hampton, Va.

NATIONAL AERONAUTICS AND SPACE ADMINISTRATION

WASHINGTON August 1962

NATIONAL AERONAUTICS AND SPACE ADMINISTRATION

TECHNICAL NOTE D-1368

STUDY OF UMBRELLA-TYPE ERECTABLE PARABOLOIDAL SOLAR CONCENTRATORS FOR GENERATION OF SPACECRAFT AUXILIARY POWER

By William D. Nowlin and Harold E. Benson

L
1
9
4
5

SUMMARY

An investigation was made of some aspects of erectable umbrella-type paraboloidal solar-energy concentrators for use in spacecraft auxiliary power systems. An analysis is presented for the design of concentrators employing radial ribs and membrane-type coverings. The rib stiffness necessary to give a desired parabolic curvature upon erection is determined.

Rib contour measurements were made in an upright and inverted position on an experimental 10-foot-diameter concentrator giving a focal length of 30.78 inches and 30.6 inches, respectively, as compared with a design focal length of 30 inches. Calorimetric tests employing spherical heat receivers showed a maximum geometrical concentrator efficiency of 75.3 percent with a concentration ratio of 92.2 at a focal length of approximately 30.5 inches.

Within the scope of this investigation, it was found that, as the concentrator size increases, the weight per unit projected area increases, time to damp to one-half amplitude increases, and the natural frequency decreases. Umbrella-type solar concentrators appear to be feasible for power conversion systems using low concentration ratios; however, for large concentrators the time required to damp out disturbances may be a problem.

INTRODUCTION

Solar energy as a source of auxiliary power for satellites or spacecraft appears desirable since it is readily available above the earth's atmosphere. The concentration of solar electromagnetic energy upon a heat receiver produces high temperatures which can be utilized in devices for the conversion of heat energy to a more useful form, electricity. Devices

such as thermoelectric converters, thermionic converters, and heat engines driving electric generators can be used with solar concentrators. Capabilities of these systems are presented in references 1 and 2.

The concentration of solar energy can be accomplished by use of an oriented paraboloidal reflector, which focuses the sun's energy on a heat receiver. A paraboloidal concentrator can be made with lightweight ribs supporting a reflecting membrane similar to a common umbrella. It can then be folded into a compact shape for launch and later be erected into a paraboloidal shape above the earth's atmosphere.

An investigation has been made to show the feasibility of developing a simple umbrella-type solar-energy concentrator. Calorimetric tests have been conducted using a 10-foot-diameter 60-rib erectable concentrator, and the obtainable efficiencies are presented herein. The effects of vibration on this type concentrator are also presented, and a method of rib design is developed.

SYMBOLS

A	area, sq ft
A_c/A_b	concentration ratio, $\frac{\text{Frontal area of concentrator}}{\text{Surface area of heat receiver}}$
C_s	solar constant, Btu/sq ft-hr
D	diameter, ft
E	Young's modulus of elasticity of material, psi
F_n	lowest natural frequency, cps
f	focal length, ft
I	moment of inertia of a cross section
K	parabolic constant, $1/2(2f)$
k	specific heat, Btu/lb-$^{\circ}$R
M	total moment of a rib, ft-lb

$\dot{M}$ differential moment of rib

N number of ribs

Q heat flux, Btu/hr

R radius of curvature, in.

T load per inch of membrane, lb

t temperature, ^{o}R

w mass flow, lb/hr

α absorptivity

$\beta = \frac{2\pi}{N}$, radians

ϵ emissivity

γ reflectivity

θ rim angle, deg

$\tau_{1/2}$ time to damp to one-half amplitude, sec

ρ distance from focal point to surface of paraboloid, ft

σ Stefan-Boltzmann constant, 0.173×10^{-8} Btu/sq ft-hr-$^{o}R^{4}$

η efficiency of concentrator-receiver system

η_g ratio of energy incident on heat receiver to total energy that was specularly reflected from concentrator

ϕ angular errors in reflector surface, deg

x radius of concentrator

$x' = \frac{x}{2f}$

x_1 any distance from center along radius of concentrator

$x_1' = \frac{x_1}{2f}$

y	y-coordinate at station x

Subscripts:

a	absorbed
b	heat receiver
c	concentrator
g	geometrical
i	incident
u	utilized
min	minimum

CONSIDERATIONS FOR SOLAR-ENERGY CONCENTRATORS

General

An erectable solar-energy concentrator for use in space should have the following characteristics: (1) capability of being packaged and launched, (2) reliable erection system, (3) capability of functioning in a space environment under fractional g-loadings for extended periods of time, (4) lightweight, and (5) good optical qualities. The capability of being launched and the reliable erection system are prime considerations and cannot be compromised, since failure of either would mean complete failure of the mission.

The capability of the solar concentrator functioning in a space environment for extended periods of time is dependent on the hazards that may be encountered. These are sublimation of the reflector surface, erosion of the surface due to meteoroid bombardment, and sputtering of the surface due to corpuscular radiation from the sun. In order to reduce the surface erosion due to sputtering, the concentrator surface must be made of a material with a high sputtering threshold. Aluminum (ref. 3) is well suited for this purpose with a sputtering threshold of 125 volts as compared with silver and gold which have thresholds below 50 volts. From calculations by Whipple (ref. 4), the erosion of the surface from all three sources should not become important optically over a period of less than 1 year.

The solar-energy concentrator must be constructed at a minimum weight and still meet the other specifications. The weight will be

related to the optical qualities, since the size of the concentrator will be dependent upon its ability to concentrate the incident solar energy on a heat receiver to obtain a specified power output and operating temperature.

Parabolic Concentrator - Spherical Heat Receiver

The type of solar-energy concentrator under consideration is the axially symmetrical parabolic concentrator. When parallel rays strike the surface of the reflector, they are reflected so that they pass through the focal point. If a receiver is placed at the focal point, the radiant energy can be collected as heat and either stored or converted to electrical or mechanical energy.

Since the earth is not an infinite distance from the sun, the sun's rays striking the reflector will not be parallel. At the distance of the earth's orbit from the sun, the average apparent angular diameter of the sun's disk is approximately 32' of arc. The rays striking the reflector will vary from parallel by ±16' of arc. This variation causes the reflected rays to form a cone with an apex angle of 32'. In order to intercept all the reflected rays with a spherical receiver, it is necessary to have a receiver with a diameter of twice the maximum distance from the focal point to the reflector times the tangent of 16' of arc. The minimum receiver diameter which would intercept all radiant energy reflected from a perfect reflector would be

$$D_{b,min} = 2\rho \tan 16' \tag{1}$$

From the definition of a parabola

$$\rho = \frac{2f}{1 + \cos \theta} \tag{2}$$

Equation (1) becomes

$$D_{b,min} = \frac{4f \tan 16'}{1 + \cos \theta} \tag{3}$$

An increase in receiver size above this minimum will cause a decrease in the maximum obtainable temperature. The limiting factor will be the temperature at which the heat receiver must be maintained while energy is removed from the system. This effect can be shown in the following

energy relation:

$$\frac{C_s A_c \gamma \eta_g \alpha_b - Q_u}{A_b \sigma \epsilon_b} = t_b^4 \tag{4}$$

where Q_u is the amount of energy taken from the heat receiver, A_c is the frontal area of the concentrator, and A_b is the surface area of the heat receiver. The geometrical efficiency η_g in equation (4) cannot be determined until the concentrator is constructed and tested. Figure 1 shows the ratio of energy removed from heat receiver to the total energy available from the sun $Q_u/C_s A_c$ for various concentration ratios and temperatures, where γ is assumed to be 0.8 and η_g, α_b, and ϵ_b are assumed to be 1.0.

Since the focal length is related to the concentrator diameter and rim angle by the expression

$$D_c = 4f \tan \frac{\theta}{2} \tag{5}$$

the minimum receiver diameter for a given concentrator diameter $\frac{D_{b,min}}{D_c}$ can be found by combining equations (3) and (5) to form

$$\frac{D_{b,min}}{D_c} = \frac{\tan 16'}{\sin \theta} \tag{6}$$

This relation is plotted in figure 2 and shows that the minimum $\frac{D_{b,min}}{D_c}$ ratio occurs when the concentrator has a rim angle of 90°, with the assumption that a spherical heat receiver is used.

The greater the distance from the concentrator surface to the heat receiver, the more perfect the reflector surface must be maintained. Since the surface angular error will cause twice the angular error of the reflected ray, the allowable surface error will then be one-half the angle whose tangent is one-half the diameter of the heat receiver divided by ρ, the radius of the parabola, minus the angular dispersion from the sun. The radius of the parabola from equation (2) is

$$\rho = \frac{2f}{1 + \cos \theta}$$

or

$$\rho = \frac{2f \tan \frac{\theta}{2}}{\sin \theta}$$

Combining this relation with equation (5) yields

$$\rho = \frac{D_c}{2 \sin \theta}$$

From this the maximum allowable error is

$$\phi = \frac{1}{2}\left[\tan^{-1}\left(\frac{D_b}{D_c} \sin \theta\right) - 16'\right] \tag{7}$$

which shows that the maximum allowable surface error is greatest at $\theta = 90^\circ$ when D_b is not a minimum.

MODELS

The solar concentrator models used in the experimental analysis were paraboloids of 90° rim angle using a spherical heat receiver as a calorimeter. A description of each model is given in table I. Two tests were made on the 10-foot-diameter concentrator shown in figure 3. The first test was made with a 1/4-mil aluminized Mylar reflector surface and the second with a 1/2-mil aluminized Mylar reflector surface. Two $2\frac{1}{2}$-foot-diameter concentrators were also tested, one with 34 ribs and one with 60 ribs.

Ribs

The concentrators tested are of the mechanically erectable rib type and are constructed with ribs similar to a common umbrella. (See fig. 3.) The ribs are of a varying cross section so that when they receive the proper bending moment they form the shape of a paraboloid. The front surface is made of aluminized Mylar which is glued to the ribs. When a bending moment is applied to the base of the ribs, the surface is stretched by the ribs to remove wrinkles and forms the desired shape. An analysis of the rib design is found in the appendix.

Erection

The erection mechanism is shown in figure 4. Gas is let into the cylinder under pressure and forces the piston forward; the ribs are thereby forced to rotate outward around a retainer ring through the ribs at the hub of the housing. When the ribs are rotated to the open position, the cam on which the piston has been acting rides up on the piston and locks.

The erected concentrator becomes a comparatively rigid structure which will require no gas to hold its shape. It is capable of withstanding moderate tracking accelerations and will return to a paraboloidal shape if it is deformed to an extent less than the yielding point of the ribs or if the Mylar has not been torn. Tearing of the Mylar would leave no restraining force on the ribs and the concentrator would distort.

Membrane

When the concentrator is fabricated, the membrane develops wrinkles and loose sections due to the difficulty in working with materials of 1/2-mil thickness. These wrinkles and loose sections would reduce the efficiency considerably if they were not removed. Mylar will shrink when heated to between 180° F and 200° F (ref. 5) and this characteristic can then be used to eliminate loose sections and remove wrinkles. The temperature of the reflector surface is brought to a high enough level to cause shrinkage by forcing hot air over the rear surface of the concentrator; the surface shrinks and the loose sections are removed. This effect can be seen by comparing figures 3 and 5, where figure 5 is as the surface of the 10-foot-diameter concentrator appears after fabrication and figure 3 is the concentrator after being heated. The wrinkles will not return upon folding and reopening of the concentrator if no creases are put in the surface.

The effects of temperature rise on the surface of the concentrator are not a problem in ground testing but should be taken into account in operation in a space environment. No tests were conducted to determine the loss in efficiency resulting from allowing the Mylar to become heated; however, indications are that allowing the temperature to rise above 180° F will change the shape by causing continued shrinkage of the reflector surface and thereby causing the concentrator to deform. From reference 5, Mylar will shrink as much as 4 percent if the temperature is allowed to remain at 300° F for an extended period of time and the tensile strength will be about one-half the original value. Since the paraboloidal shape is maintained by tension in the surface, this combined shrinkage and loss of strength would probably deform the concentrator and cause a loss in

efficiency. From these considerations, it is necessary that the rear surface have such an emissivity as to keep temperature of the concentrator below 180° F.

The effect of space environment on the Mylar rear surface has not been fully investigated, but it is known that exposure to sunlight will deteriorate Mylar and cause it to become brittle. Even though the concentrator will always be oriented with the sun, the reflected solar energy from the earth will affect the Mylar and it must therefore be protected by a coating having desirable emissivity characteristics and resistance to the space environment. Some radiation will penetrate the aluminum surface and cause it to deteriorate and lose strength; however, the time necessary to cause an appreciable change in the concentrator has not been determined.

APPARATUS AND PROCEDURE

Contour Measurements

Contour measurements were made of the ribs of the 10-foot-diameter concentrator to determine how well the ribs followed the design shape. The rib contours of the collector were obtained by mechanical measurements with the equipment shown in figure 6. The projected area of the collector was divided into 10 equal concentric areas and the probes were located at the midpoint of the width of the concentric areas. The probes were lowered until a rib of the collector was touched and a dial gage used to measure the probe position. Measurements of the collector are believed to be accurate to ±1/100 inch. Every fifth rib was measured with the collector in an upright and inverted position. The collector was tilted at 34.5° and every fifteenth rib was measured. The focal point of the best fitting parabola was obtained by applying the method of least squares to the data obtained from the different positions.

Vibration Measurement

Vibration tests were conducted on a 30-inch-diameter 34-rib umbrella and the 10-foot-diameter 60-rib umbrella in air and in a vacuum. A rib was depressed with a solenoid, the vacuum chamber pumped down, and the solenoid released. High-speed movies were taken of a pointer, attached to the tip of a rib, against a grid background and were used to determine the amplitude and frequency of vibration.

Surface Optical Characteristic Measurements

The reflectivity of the concentrator surface was determined by taking samples from the concentrator surface and checking them in a spectrophotometer. The reflectivity of the surface used in the initial test was found to be low because of excessive handling prior to the calorimetric test. The reflectivity of this surface is plotted in figure 7. The surface of the concentrator was replaced by a second surface and samples of the second cover tested. The reflectivity of the new surface is also plotted in figure 7.

The solar radiation at the test site appears to be equivalent to solar radiation available with an optical air mass of 2, as found in reference 6, and is plotted in figure 8. The amount of solar energy reflected from the concentrator surface was found by first multiplying the energy available by the reflectance at various wavelengths as shown in figure 8. The area under each curve was integrated and the reflectivity of the surface to solar radiation is found by dividing the area under the curve for each surface by the area under the solar spectrum curve.

The absorptivity of the heat receiver was found by coating a sample with the same flat black paint as the heat receiver and measuring the reflectivity with a spectrophotometer. This effect is shown in figure 7. Since there is no transmittance for the heat receiver, the absorptivity is found to be 1 minus the reflectivity.

Calorimetric Test

The calorimetric efficiency tests for the 10-foot solar concentrator were conducted in the solar research facility shown in figure 9. This facility is constructed with a door at 37° to the ground, which corresponds approximately to the latitude of the Langley Research Center. This value allows for maximum sunlight to enter the facility during all seasons of the year as shown in figure 10.

The concentrator was mounted on an equatorial mount with a clock drive for maintaining alinement with the sun as shown in figure 11. The alinement is checked by an elbow telescope mounted parallel with the optical axis of the concentrator. Water is pumped through the heat receiver as shown in the schematic figure 12. The water enters the system at approximately the same temperature as the surrounding air, and a differential thermocouple measures the rise in temperature after passing through the heat receiver. The flow is measured by a turbine flowmeter located in the inlet water line. The incident solar energy is measured with a pyrheliometer located on the longitudinal axis of the mount. The flow rate, differential temperature, and amount of incident solar energy are recorded on a permanent record. The overall efficiency of the

concentrator-heat receiver system was determined from the relation

$$\eta = \frac{kw\ \Delta t}{A_c Q_i}$$

where Δt is kept small so convection and radiation losses can be ignored. The actual geometrical efficiency is determined by dividing the overall efficiency by the reflectivity of the concentrator surface and the absorptivity of the heat-receiver surface. The experimental focal point was determined by moving the heat receiver along the focal axis in and out past the design focal point and determining efficiency throughout the range covered.

Three heat receivers having diameters of 3 inches, 6.25 inches, and 12 inches were used in the test to show the effect of concentration ratio on concentrator efficiency.

Calorimetric tests were also conducted for two 30-inch-diameter concentrators prior to construction of the 10-foot-diameter concentrator to see whether the rib-type concentrator would be practical. Tests on the 30-inch concentrator were conducted with the concentrator on a manual equatorial mount. One 30-inch concentrator was tested with a 2.7-inch-diameter spherical heat receiver, the other used a 1.75-inch-diameter spherical heat receiver. Water was passed through the heat receiver as in the test on the 10-foot-diameter concentrator and the temperature change measured by differential thermocouples on the inlet and outlet water supplies. The flow rate was measured by allowing the water to flow into a graduated cylinder and timing the flow with a stopwatch, and the solar intensity was measured with a calibrated thermopile.

RESULTS AND DISCUSSION

Rib Analysis

The discussion of the weight of the membrane and ribs of the umbrella concentrator will be based on the design procedure presented in the appendix. As pointed out in the appendix, the design of the concentrator is based on the assumption of a constant circumferential membrane stress. If the membrane thickness is held constant as the collector size is varied, the design circumferential stress in the membrane would be constant and the weight of the membrane per unit projected area of the concentrator would be constant. To determine the weight per unit projected area for the ribs, the moment equation from the appendix

$$M = \frac{T(2f)^2}{2} \sin \frac{\beta}{2} \left\{ \frac{x'}{2}\left(x'^2 + 1\right)^{3/2} - x'\left(x_1'^2 + \frac{1}{4}\right)\left(x'^2 + 1\right)^{1/2} \right.$$

$$- \left(x_1'^2 + \frac{1}{4}\right) \log \left[\frac{x' + \left(x'^2 + 1\right)^{1/2}}{x_1' + \left(x_1'^2 + 1\right)^{1/2}} \right] - \frac{1}{2} x_1' \left(x_1'^2 + 1\right)^{3/2}$$

$$\left. + x_1'\left(x_1'^2 + \frac{1}{4}\right)\left(x_1'^2 + 1\right)^{1/2} \right\}$$

is substituted in the equation for the moment of inertia of the rib cross section

$$I = \frac{MR}{E}$$

Once the material and shape of the rib cross section are selected, the taper of the ribs is set and the volume of the rib may be determined. The volume of the rib times the number of ribs and the density of the material divided by the projected area of the concentrator will give the weight per unit projected area for the ribs.

It was shown in reference 7 that an increase in the number of ribs will increase the concentrator efficiency. Also for concentrators with more than 30 ribs, it can be seen from equation (A11) that the weight per unit projected area does not vary with the number of ribs. Thus, the use of more ribs will increase the concentrator efficiency with no weight penalty. Figure 13(a) shows the effect on rib weight of two rib cross sections: a square section at the rib root that holds the width constant and tapers in depth only, and an I-section where the width equals the depth and both width and depth taper. For a specific material and rib cross-sectional shape, the weight per unit projected area of the ribs varies as the square root of the concentrator diameter. Figure 13(b) shows the weight per unit projected area for solid ribs with a square section at the root that holds the width constant and tapers in depth for several different materials. Data for these plots were obtained by assuming a stress level of 800 pounds per square inch in the membrane.

Since the weight per unit projected area of the membrane is constant and the weight per unit projected area of the ribs increases as the square root of the concentrator diameter, the weight of the membrane becomes proportionately smaller as concentrator size increases. The effect of the membrane-rib proportions on the vibration of the concentrator is discussed in a following section.

Contour Measurements

The results of the contour measurements of the ribs of the 10-foot-diameter concentrator are summarized in figure 14 where the differences between the measured ordinate of the ribs and the corresponding ordinate of the design parabola are plotted against the concentrator abscissa. The ordinate scale has been magnified 10 times for clarity.

Data obtained from measuring the concentrator in the upright position are presented in figure 14(a) for the differences between the design parabola $x^2 = 120y$ and the best fitting rib, worst fitting rib, and the average of all the ribs measured. The inner area of the concentrator followed the design parabola fairly well but then fell progressively farther away until near the rim of the concentrator where a circumferential string tended to pull the ribs back into position. The method of least squares was applied to the data to determine the parabola that would best fit the measured contours of the ribs. The differences between this parabola $x^2 = 123.13y$ and the average of all the ribs measured are shown at the bottom of figure 14(a). The focal length of $x^2 = 123.13y$ is 30.78 inches compared with 30.00 inches for the design parabola.

Since the ribs fell below the design parabola, the concentrator was measured in an inverted position to determine the effect of gravity on the shape of the concentrator. Data obtained from these measurements are shown in figure 14(b). There was very little difference in the shape of the concentrator between the upright and inverted positions. The maximum change in a rib ordinate was 0.35 inch. Applying the method of least squares to the data obtained from inverted position gave $x^2 = 122.40y$ which has a focal length of 30.6 inches.

Data obtained from measuring the concentrator while tilted 34.5° are shown in figure 14(c). The differences of the ordinates are shown for four ribs. When one faces the concentrator, 0° is the 12 o'clock position, 90° is 3 o'clock, 180° is 6 o'clock, and 270° is 9 o'clock. The greatest change in the shape of the ribs is between the rib at 0° and the rib at 180°. Use of the method of least squares gave focal lengths of 30.32 inches for the 0° rib and 31.84 inches for the 180° rib. Averaging all the ribs measured gives $x^2 = 123.72y$ with a focal length of 30.93 inches.

Vibrations

By using the free-vibration method described under "Apparatus and Procedure" the natural frequency and time to damp to one-half amplitude were obtained for the 30-inch- and 10-foot-diameter concentrators. The concentrators were vibrated at atmospheric pressure and in vacuum chambers

at reduced pressure (0.1 mm Hg pressure for the 30-inch concentrator and 27 mm Hg pressure for the 10-foot concentrator). The data were extrapolated to obtain the frequency of the concentrators in a perfect vacuum and are presented in table II. The natural frequency of the cantilever ribs of the 30-inch- and 10-foot-diameter concentrators with the membrane detached is included in the table. It appears from comparisons of the natural frequencies that for the 30-inch concentrator, where the membrane is 36 percent of the weight of the membrane and ribs, the rib frequency is different from the concentrator frequency. However, the membrane of the 10-foot concentrator is less than 2 percent of the weight of the membrane and ribs, and the rib and concentrator frequencies are approximately the same. As the size of the concentrator is increased, the membrane weight becomes a smaller percentage of the total; therefore, the natural frequency of a large umbrella concentrator in space can probably be approximated by the natural frequency of a rib alone measured in air.

An example of variation of rib frequency against size is shown in figure 15 for aluminum ribs with square cross sections at the hub and tapering in depth only. For solar concentrators built according to the design procedure in the appendix, rib frequency varies as diameter to the -1.25 power. The effect of the number of ribs is also shown.

Both the 30-inch- and 10-foot-diameter concentrators took about the same number of cycles to damp to one-half amplitude. If this holds true with larger sizes, since the frequency varies as the diameter to the -1.25 power, the time to damp to one-half amplitude may become a problem in space operations.

Surface Optical Characteristics

The reflectivity measurements of the first concentrator covering for the 10-foot concentrator showed that the specular reflectivity to the sun's energy of the aluminized Mylar was 0.64. The surface was 1/4-mil-thick Mylar with an aluminum vapor coating probably less than 2,000 angstroms thick. This low value of reflectivity was due to repeated handling and cleaning of the concentrator prior to the test and continued opening and closing of the concentrator to test the erecting mechanism. The surface was then replaced with a 1/2-mil-thick Mylar film which also had an approximately 2,000-angstrom-thick vapor coating of aluminum. The reflectivity of the second surface was found to be 0.83.

The reflectivity of the heat receiver was found to be approximately 0.04 over the entire available range of solar energy and yields an absorptivity of 0.96 for an optical air mass of 2.

Calorimetric Tests

The maximum overall efficiency of the 10-foot-diameter concentrator-receiver system with the 1/4-mil surface using a 6.25-inch-diameter heat receiver of concentration ratio 92.2 was found to be 46 percent. The geometrical efficiency, an allowance being made for reflectivity of the concentrator surface and absorptivity of the heat receiver, was 74.8 percent. The tests were rerun with the 1/2-mil surface on the concentrator, and the maximum overall efficiency was found to be 60 percent, a value giving a geometrical efficiency of 75.3 percent.

The test with the 12-inch heat receiver of concentration ratio 25 showed a maximum geometrical efficiency of 97.3 percent, and the 3-inch heat receiver of concentration ratio of 400 had a maximum geometrical efficiency of 26.2 percent. The geometrical efficiency plotted against distance along the optical axis is shown in figure 16 and shows that the focus for maximum efficiency is longer than design length and is at approximately $30\frac{1}{2}$ inches. These values of geometrical efficiency were used in equation (4) and the ratios of usable energy to available energy obtained are shown in figure 17. These data can be compared with values of a geometrically perfect concentrator in figure 1.

The geometrical efficiency of the 12-inch heat receiver was lower than expected when the center of the sphere was located at a focal length of 30.5 inches. (See fig. 16.) It was found that, when the main concentration of reflected light struck the equator of the sphere, the section began to heat up rapidly. This effect was due to poor circulation of the water in the upper portion of the sphere and a heavy weld at the equator. This condition caused radiation and convection losses and lowered the efficiency. Since the concentrator was not designed for a heat receiver of this size, the sphere was not redesigned to eliminate this condition. Another factor which would lower the efficiency of the concentrator was the presence of surface wrinkles which could not be removed from the joints where the gores were bonded together.

The tests on the 2.5-foot concentrators showed that the overall efficiency was 56 percent for both the 34-rib model with a 2.7-inch heat receiver and the 60-rib model with a 1.75-inch heat receiver. No further tests were conducted with the smaller models since the 10-foot-diameter concentrator would give more realistic data.

CONCLUDING REMARKS

The results of the experimental tests and theoretical analysis on erectable umbrella-type paraboloidal solar-energy concentrators may be summarized as follows:

1. With an increase in size of the concentrator, the following effects occur: the weight per unit projected area increases; the time to damp to one-half amplitude increases; and the lowest natural frequency of the concentrator decreases.

2. An increase in the number of ribs has the following effects: for 30 ribs or more, the rib weight per unit projected area will remain approximately constant; the natural frequency of the concentrator will decrease slightly; and the time to damp to one-half amplitude may be further increased.

3. The location of the focal point found by contour measurements and calorimetric tests showed close agreement, and the efficiency did not drop appreciably as the heat receiver was moved for short distances along the optical axis.

4. The efficiency of the concentrator decreases as the concentration ratio is increased.

5. The 60-rib concentrator with the design discussed in this paper could be used for conversion devices which use a low concentration ratio; however, for large concentrators the time to damp out disturbances may be a problem.

Langley Research Center,
National Aeronautics and Space Administration,
Langley Station, Hampton, Va., May 1, 1962.

APPENDIX

DESIGN PROCEDURE

The design of the umbrella concentrator is based on the assumption of a constant circumferential membrane stress, with the cross section of the ribs varied so that their deflection curve is the desired parabolic shape. The radial stress in the membrane is assumed to be zero. Referring to figures 18(a) and 18(b), T is the circumferential load per inch of the membrane which is resolved into the radial component by

$$T \sin \frac{\beta}{2} \tag{A1}$$

where

$$\beta = \frac{2\pi}{N}$$

The membrane is on both sides of the rib; therefore, the load on one rib is equal to

$$2T \sin \frac{\beta}{2} \tag{A2}$$

Now in plane AOC (fig. 18(c)), the load based on the unit length in the OC direction is

$$2T \sin \frac{\beta}{2} \sqrt{1 + \left|\frac{dy}{dx}\right|^2}\, dx \tag{A3}$$

where $\sqrt{1 + \left|\frac{dy}{dx}\right|^2}\, dx$ is the surface element being acted upon by this load. The differential moment of this differential load about x_1 is

$$\dot{M} = 2T \sin \frac{\beta}{2} \sqrt{1 + \left|\frac{dy}{dx}\right|^2} \left(y - y_{x_1}\right) dx \tag{A4}$$

The total moment resulting from all loads between x_1 and x where x is the total length or radius of the concentrator and x_1 is any point from the axis OA along the radius is

$$M = 2T \sin \frac{\beta}{2} \int_{x_1}^{x} \left(1 + \left|\frac{dy}{dx}\right|^2\right)^{1/2} \left(y_x - y_{x_1}\right) dx \tag{A5}$$

It is desirable that $y(x)$ be a parabola; therefore

$$y = Kx^2 \tag{A6}$$

Taking the derivative with respect to x yields

$$\frac{dy}{dx} = 2Kx \tag{A7}$$

and

$$y_{x_1} = Kx_1^2 \tag{A8}$$

where $K = \frac{1}{2(2f)}$ and f is the focal length. By substituting equations (A6), (A7), and (A8) into equation (A5), the following relation is obtained

$$M = 2T \sin \frac{\beta}{2} \int_{x_1}^{x} \left(1 + 4K^2x^2\right)^{1/2} \left(Kx^2 - Kx_1^2\right) dx \tag{A9}$$

Rearranging equation (A9) gives

$$M = 4TK^2 \sin \frac{\beta}{2} \left[\int_{x_1}^{x} x^2 \left(\frac{1}{4K^2} + x^2\right)^{1/2} dx - x_1^2 \int_{x_1}^{x} \left(\frac{1}{4K^2} + x^2\right)^{1/2} dx\right] \tag{A10}$$

Integrating between the limits yields the moment

$$M = \frac{T(2f)^2}{2} \sin\frac{\beta}{2}\left\{\frac{x'}{2}\left(x'^2+1\right)^{3/2} - x'\left(x_1'^2+\frac{1}{4}\right)\left(x'^2+1\right)^{1/2}\right.$$

$$- \left(x_1'^2+\frac{1}{4}\right)\log\left[\frac{x'+\left(x'^2+1\right)^{1/2}}{x_1'+\left(x_1'^2+1\right)^{1/2}}\right] - \frac{1}{2}x_1'\left(x_1'^2+1\right)^{3/2}$$

$$\left. + x_1'\left(x_1'^2+\frac{1}{4}\right)\left(x_1'^2+1\right)^{1/2}\right\} \qquad \text{(A11)}$$

where $\frac{x}{2f}$ and $\frac{x_1}{2f}$ are replaced by x' and x_1', respectively, for simplicity.

REFERENCES

1. Fisher, J. H.: An Analysis of Solar Energy Utilization. WADC Technical Report 59-17, Vols. I and II, U.S. Air Force, Feb. 1959.

2. Von Doenhoff, Albert E., and Hallissy, Joseph M., Jr.: Systems Using Solar Energy for Auxiliary Space Vehicle Power. Rep. No. 59-40, Inst. Aero. Sci., Jan. 1959.

3. Singer, S. F.: The Effect of Meteoric Particles on a Satellite. Jet Propulsion, vol. 26, no. 12, Dec. 1956, pp. 1071-1075, 1087, 1090.

4. Whipple, Fred L.: The Meteoritic Risk to Space Vehicles. Vol. I of Vistas in Astronautics, Morton Alperin and Marvin Stern, eds., Pergamon Press (New York), c.1958, pp. 115-124.

5. Amborski, Leonard E., and Flierl, Donald W.: Physical Properties of Polyethylene Terephthalate Films. Industrial and Engineering Chemistry, vol. 45, no. 10, Oct. 1953, pp. 2290-2295.

6. Anon.: Handbook of Geophysics. Revised ed., The Macmillan Co., 1961.

7. Bond, Victor R.: Measurements and Calculations of the Effects of Distortions in the Collector Surface on Efficiencies of Umbrella-Type Solar Collectors. NASA TN D-925, 1961.

TABLE I.- DESCRIPTION OF CONCENTRATOR MODELS USED IN TESTS

Concentrator diameter, ft	Number of ribs	Rib material	Thickness of reflector surface, mil	Rim angle, deg	Weight of ribs and reflector surface, lb	Weight of erection mechanism, lb	Total weight, lb	Diameter of heat receivers used during test, in.
10	60	Aluminum	1/4	90	8.5	16	24.5	3, 6.25, 12
10	60	Aluminum	1/2	90	8.5	16	24.5	3, 6.25, 12
2.5	34	Aluminum	1/2	90	0.28	0.77	1.05	2.7
2.5	60	Magnesium	1/4	90	*0.35		0.35	1.75

*Nonerectable ribs welded to magnesium hub which is included in this weight.

TABLE II.- VIBRATION DATA FOR TWO UMBRELLA CONCENTRATORS

	30-inch-diameter concentrator	10-foot-diameter concentrator
F_n (air)	13 $\frac{\text{cycles}}{\text{sec}}$	1 $\frac{\text{cycle}}{\text{sec}}$
F_n (vacuum)	17 $\frac{\text{cycles}}{\text{sec}}$ (0.1 mm Hg)	1.85 $\frac{\text{cycles}}{\text{sec}}$ (27 mm Hg)
F_n (vacuum, perfect)	17.05 $\frac{\text{cycles}}{\text{sec}}$	1.94 $\frac{\text{cycles}}{\text{sec}}$
F_n rib (air)	12.35 $\frac{\text{cycles}}{\text{sec}}$	2.24 $\frac{\text{cycles}}{\text{sec}}$
$\tau_{1/2}$ (air)	1.06 sec	2.65 sec
$\tau_{1/2}$ (vacuum)	1.5 sec (0.1 mm Hg)	16.5 sec (27 mm Hg)

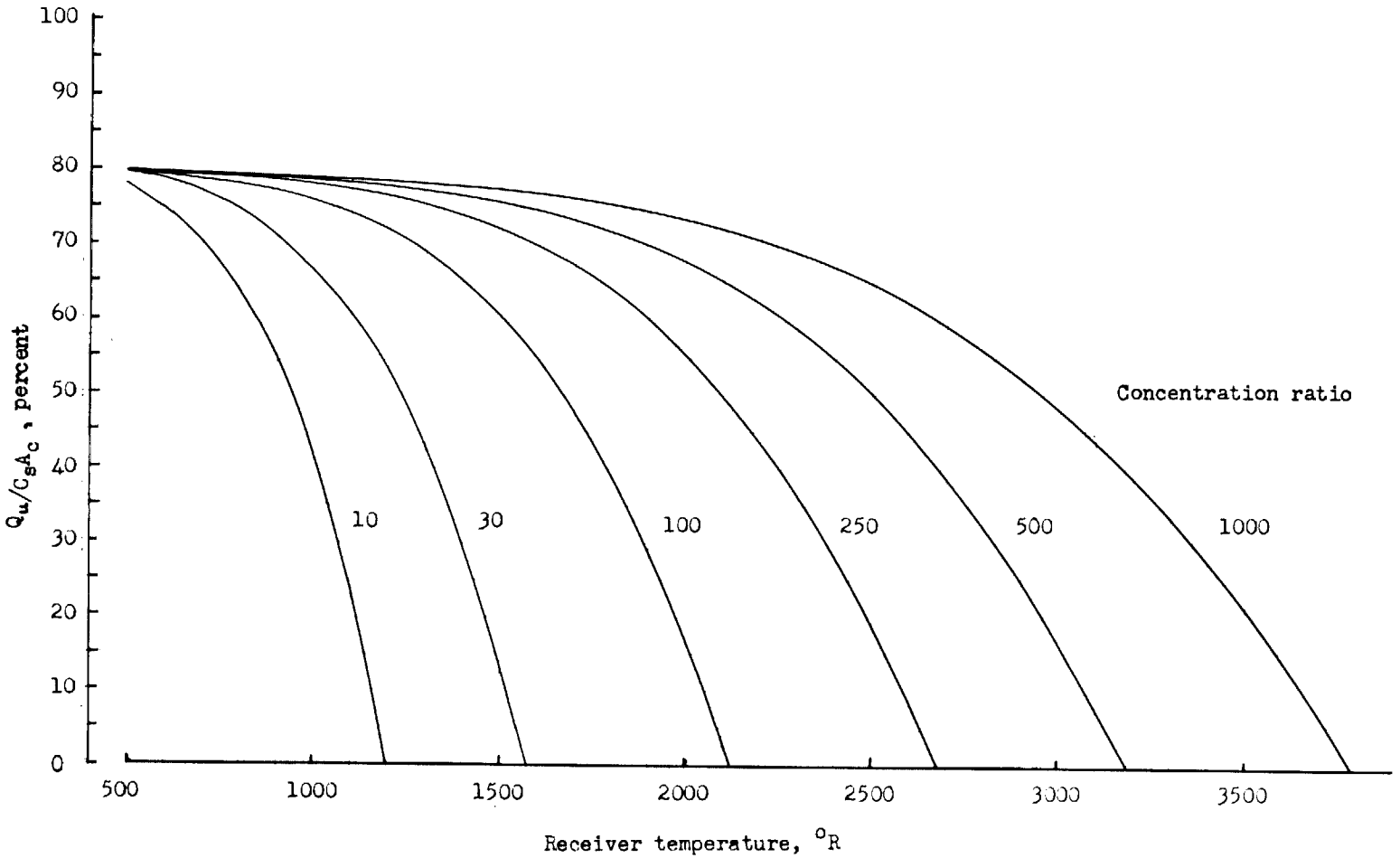

Figure 1.- Ratio of usable to available energy for various concentration ratios and receiver temperatures. $\gamma = 0.8$; $\eta_g = 1.0$; $\alpha_b = 1.0$; and $\epsilon_b = 1.0$.

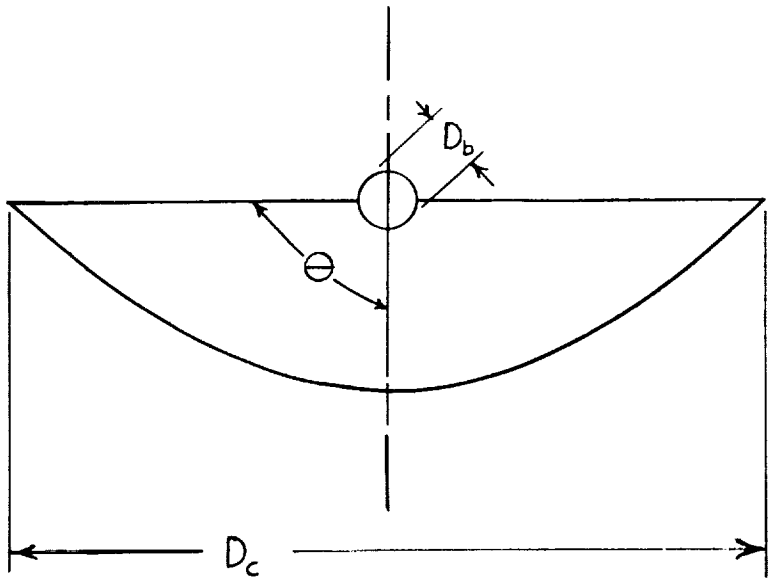

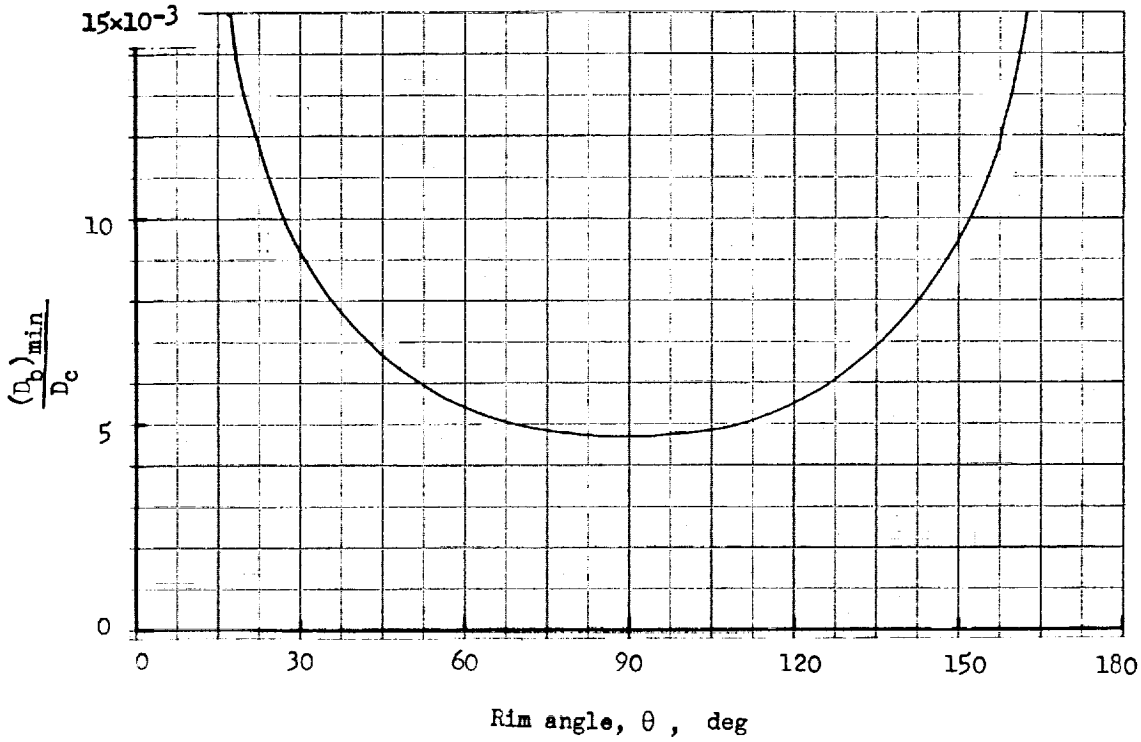

Figure 2.- Variation of ratio of minimum heat receiver to concentrator diameter with rim angle.

Figure 3.- The 10-foot-diameter concentrator after being heated. L-60-1409

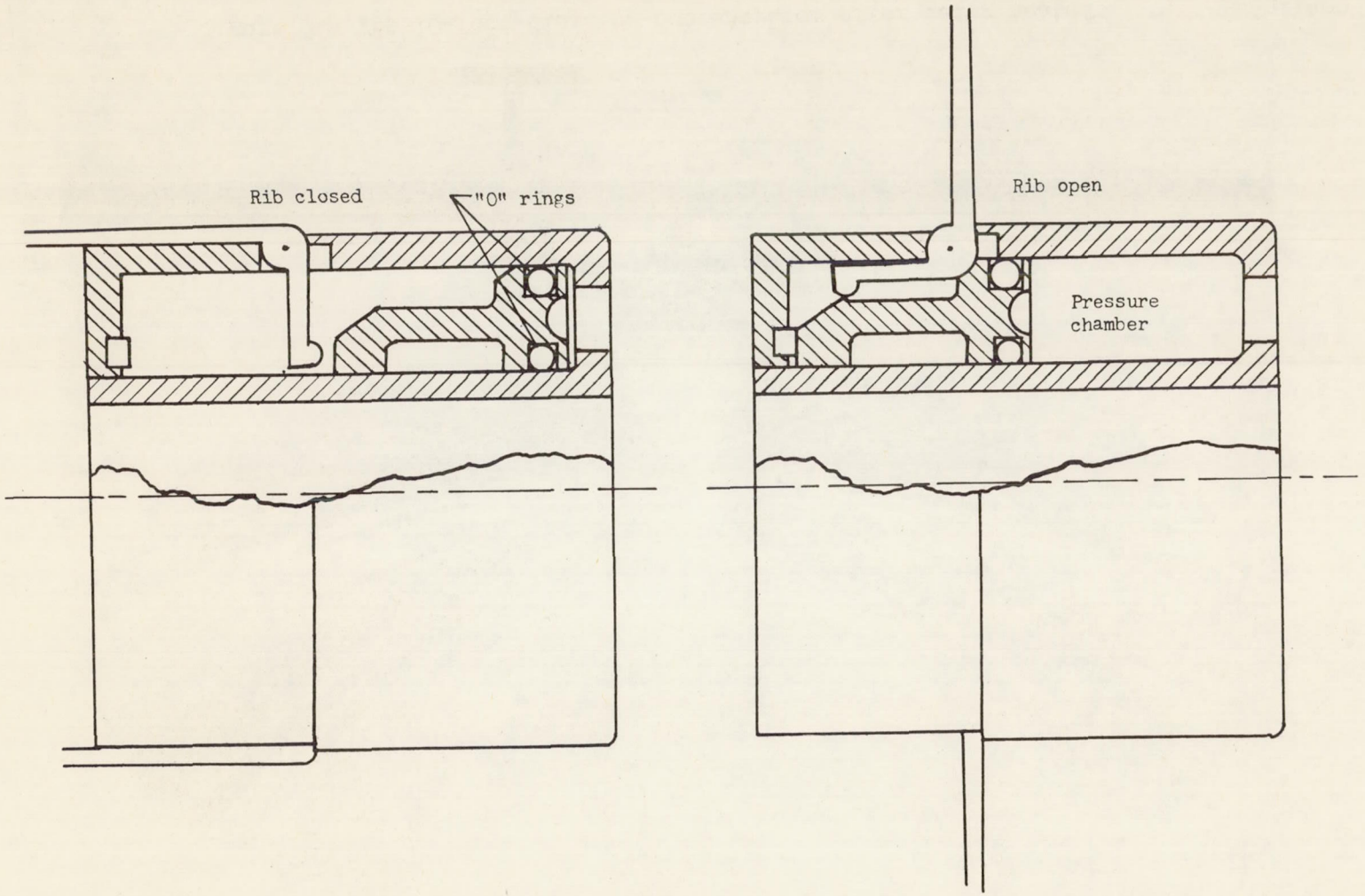

Figure 4.- Erecting mechanism for mechanically erectable solar concentrator.

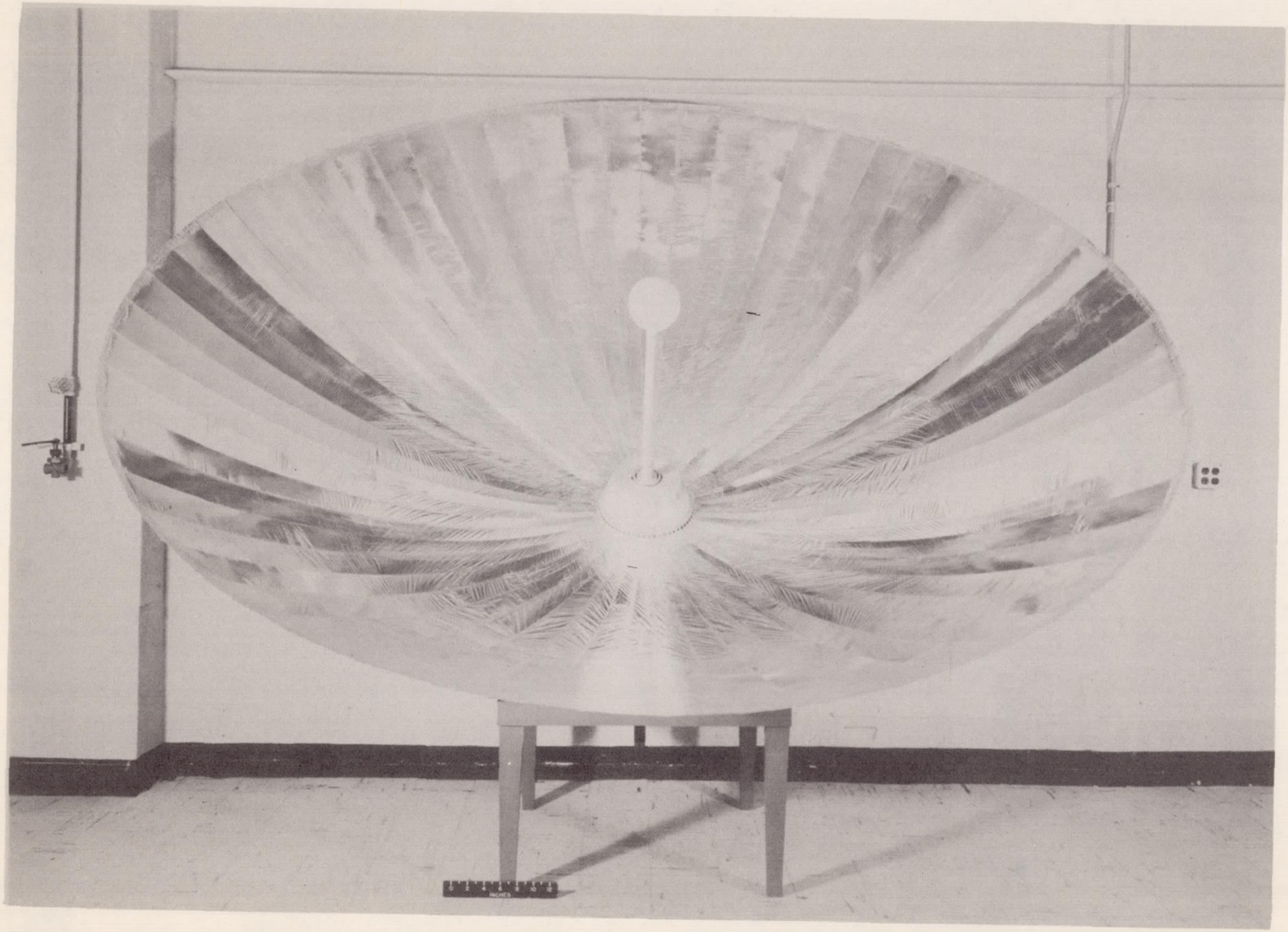

Figure 5.- The 10-foot-diameter concentrator as fabricated. L-59-8381

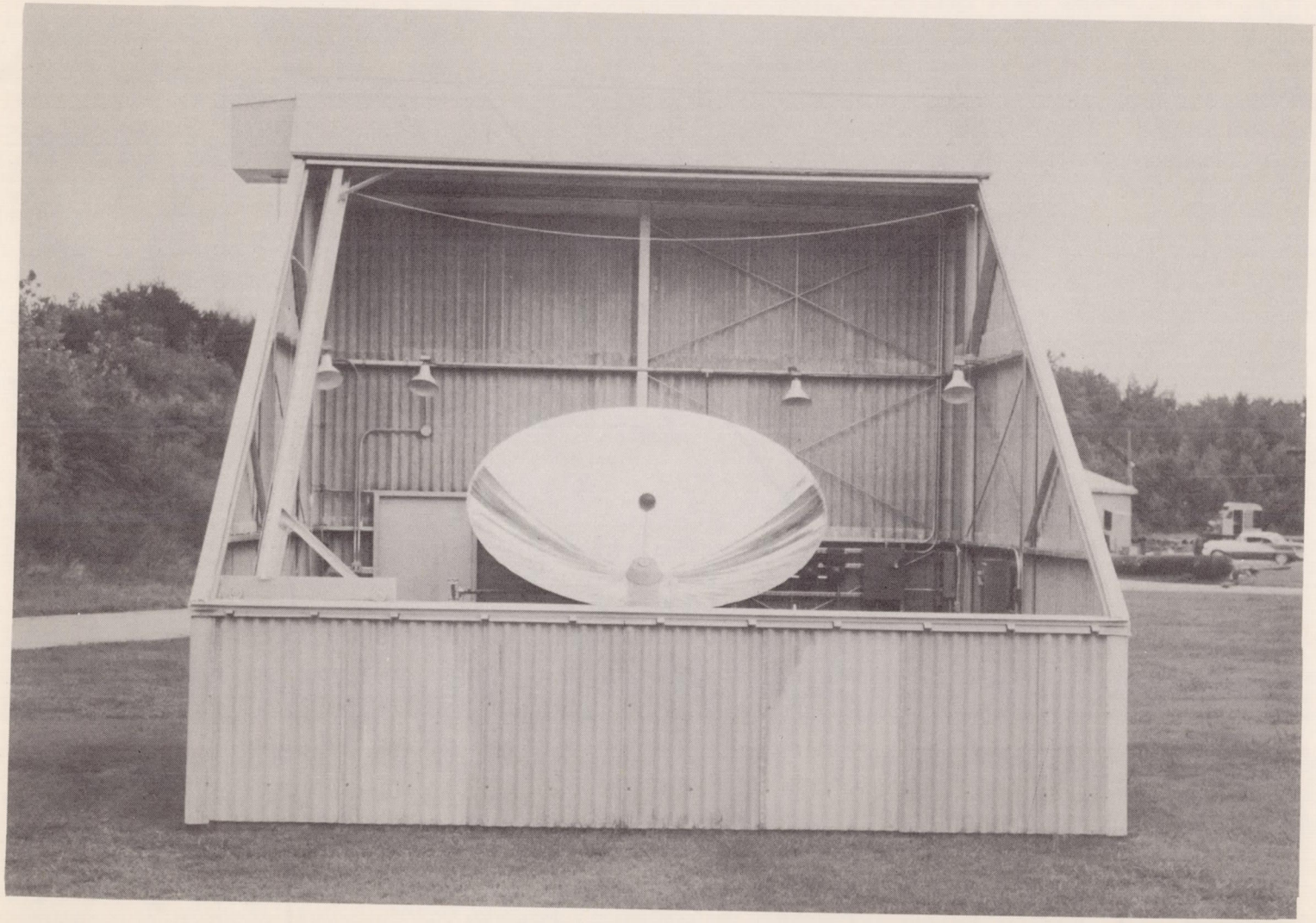

L-60-4969

Figure 9.- Solar-energy test facility with 10-foot-diameter concentrator in test position.

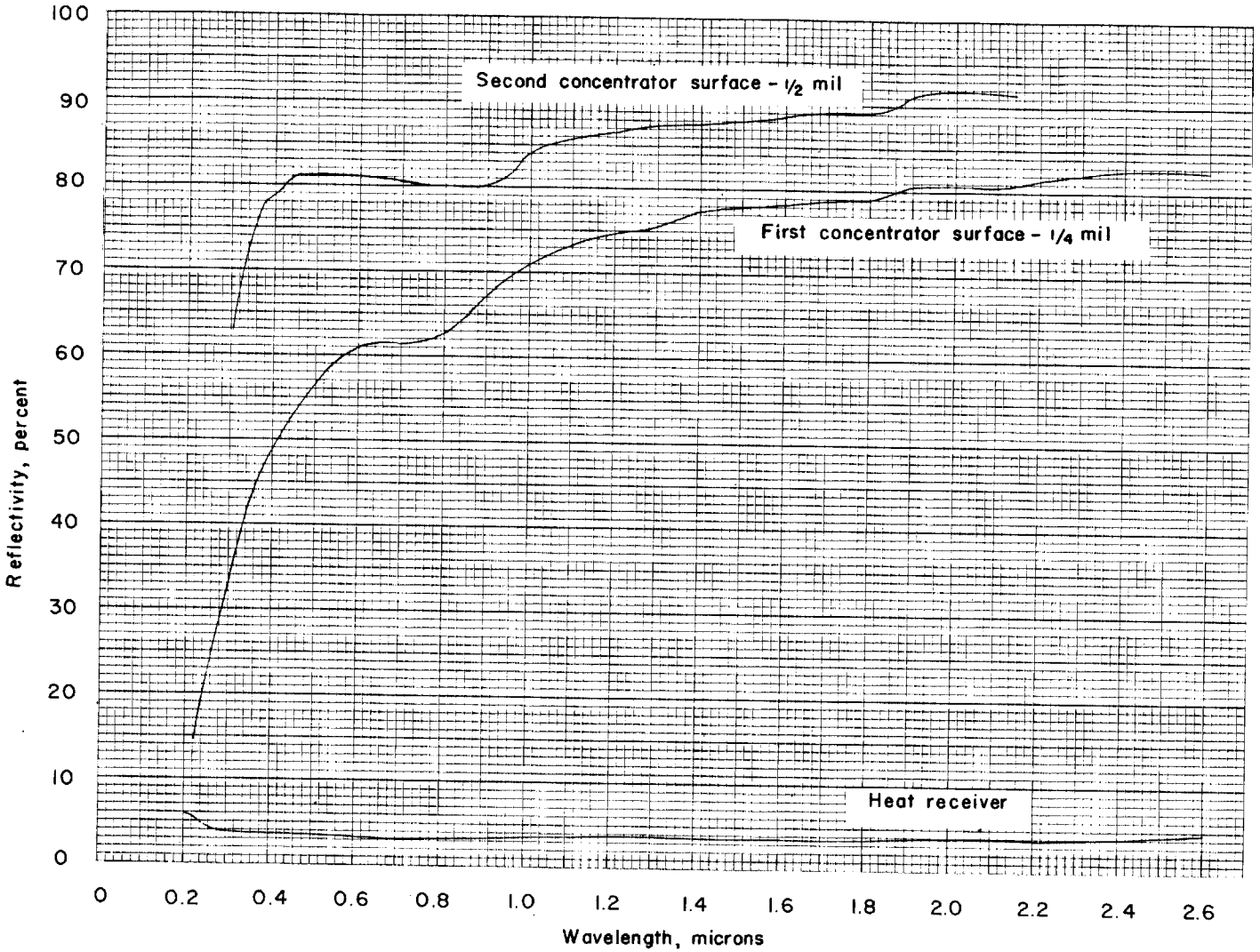

Figure 7.- Monochromatic reflectivity of concentrator-receiver components.

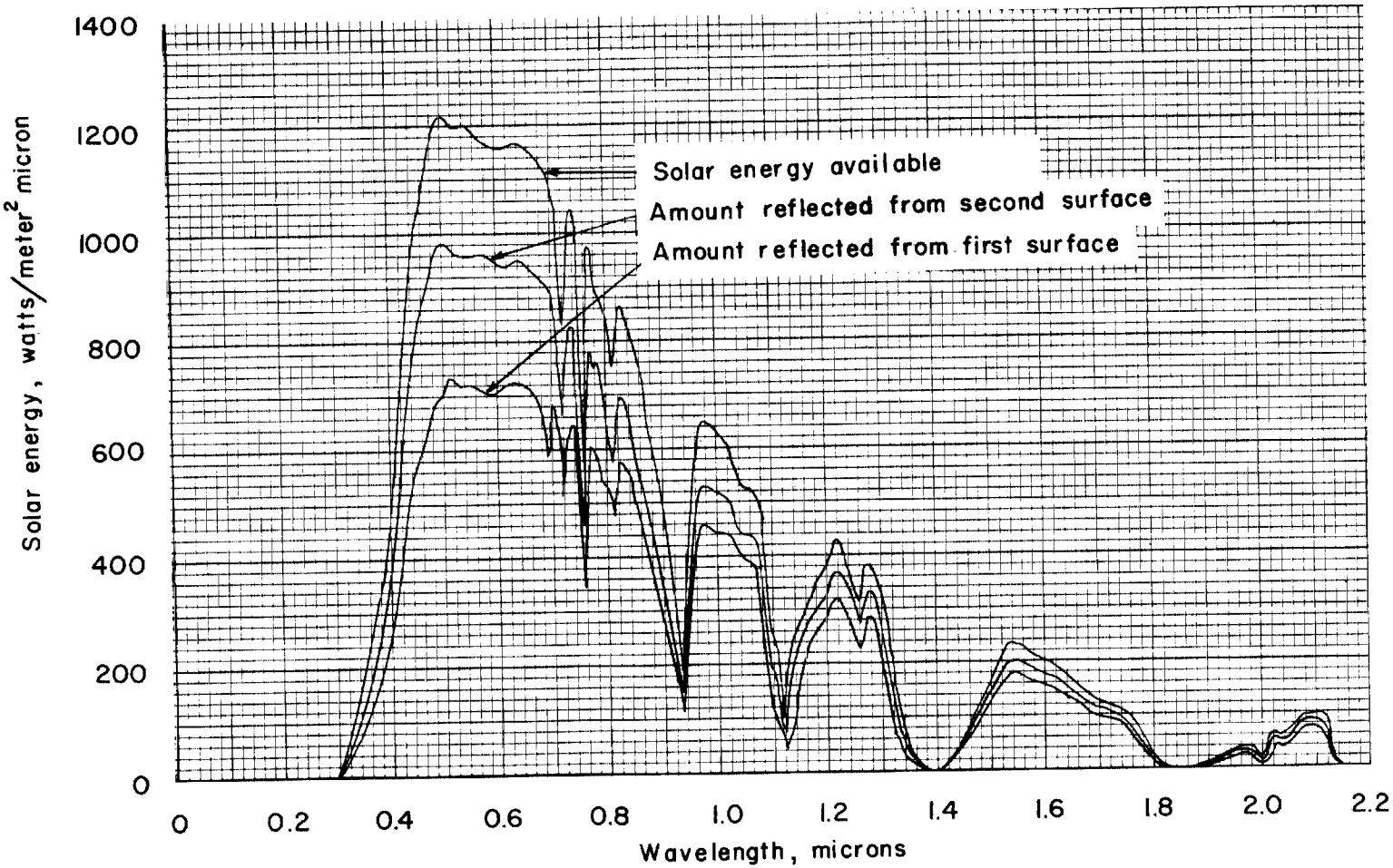

Figure 8.- Energy reflected from concentrator surface compared with available energy.

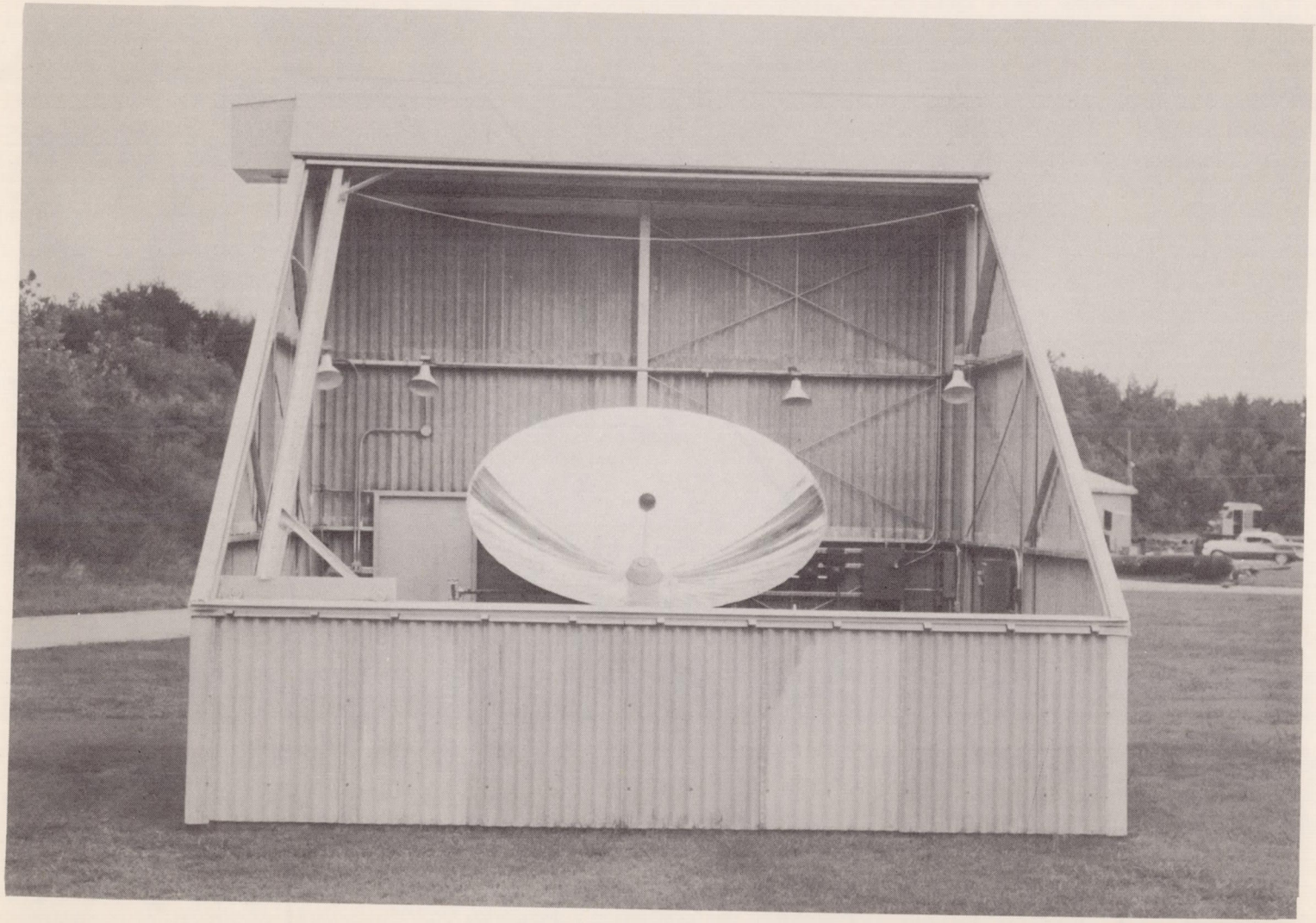

L-60-4969

Figure 9.- Solar-energy test facility with 10-foot-diameter concentrator in test position.

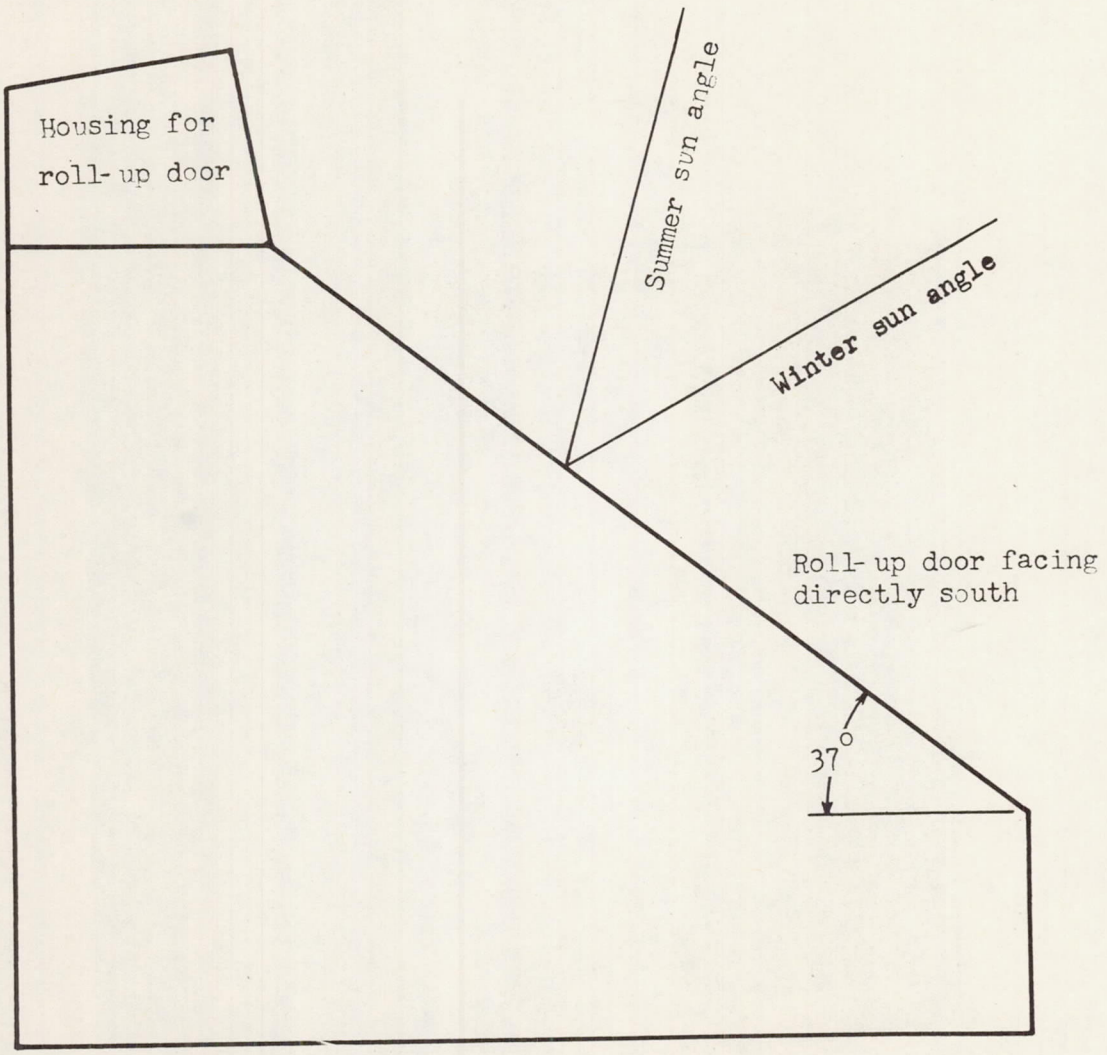

Figure 10.- Diagram showing arrangement of solar-energy concentrator test facility.

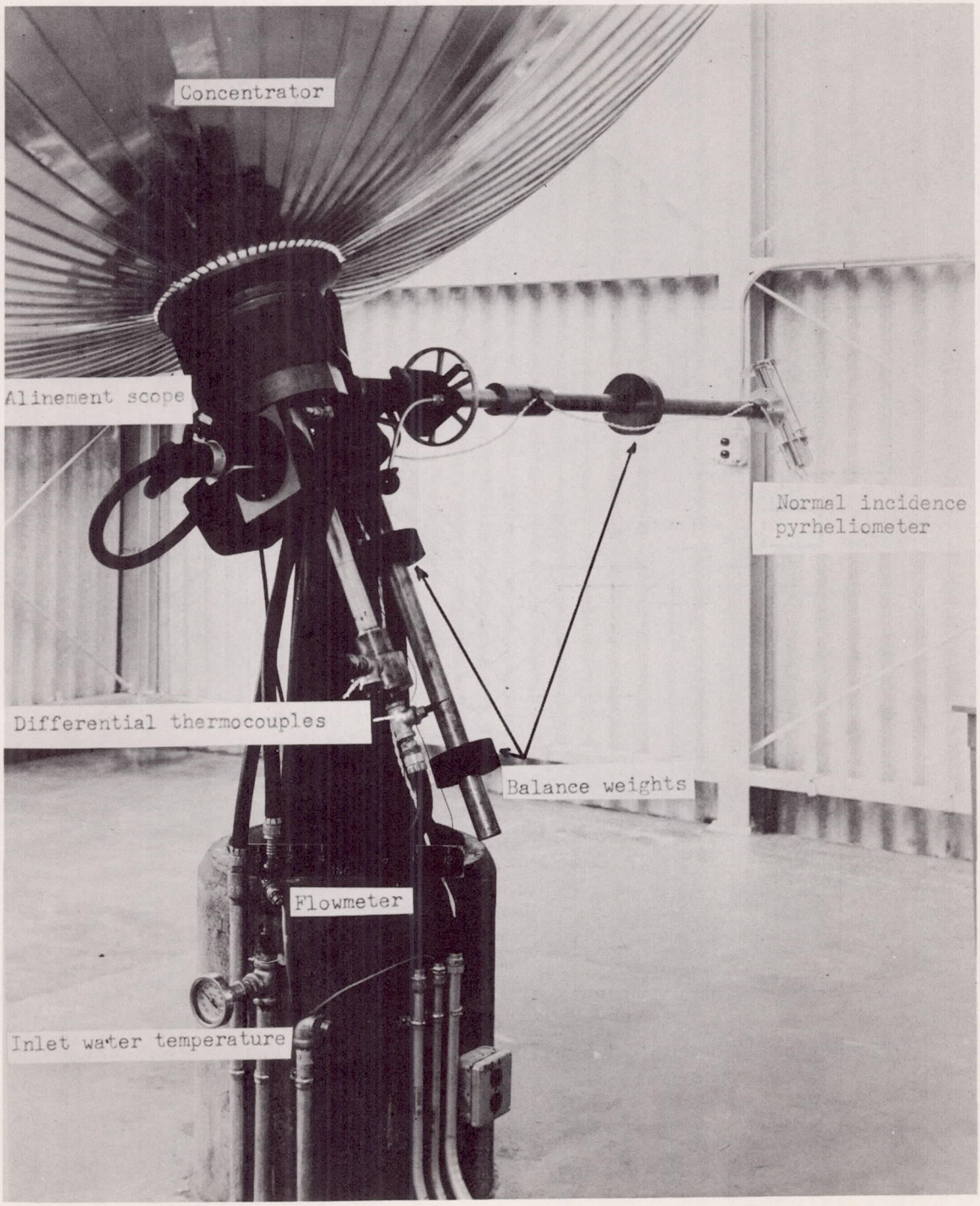

Figure 11.- Equatorial mounting. L-60-4966.1

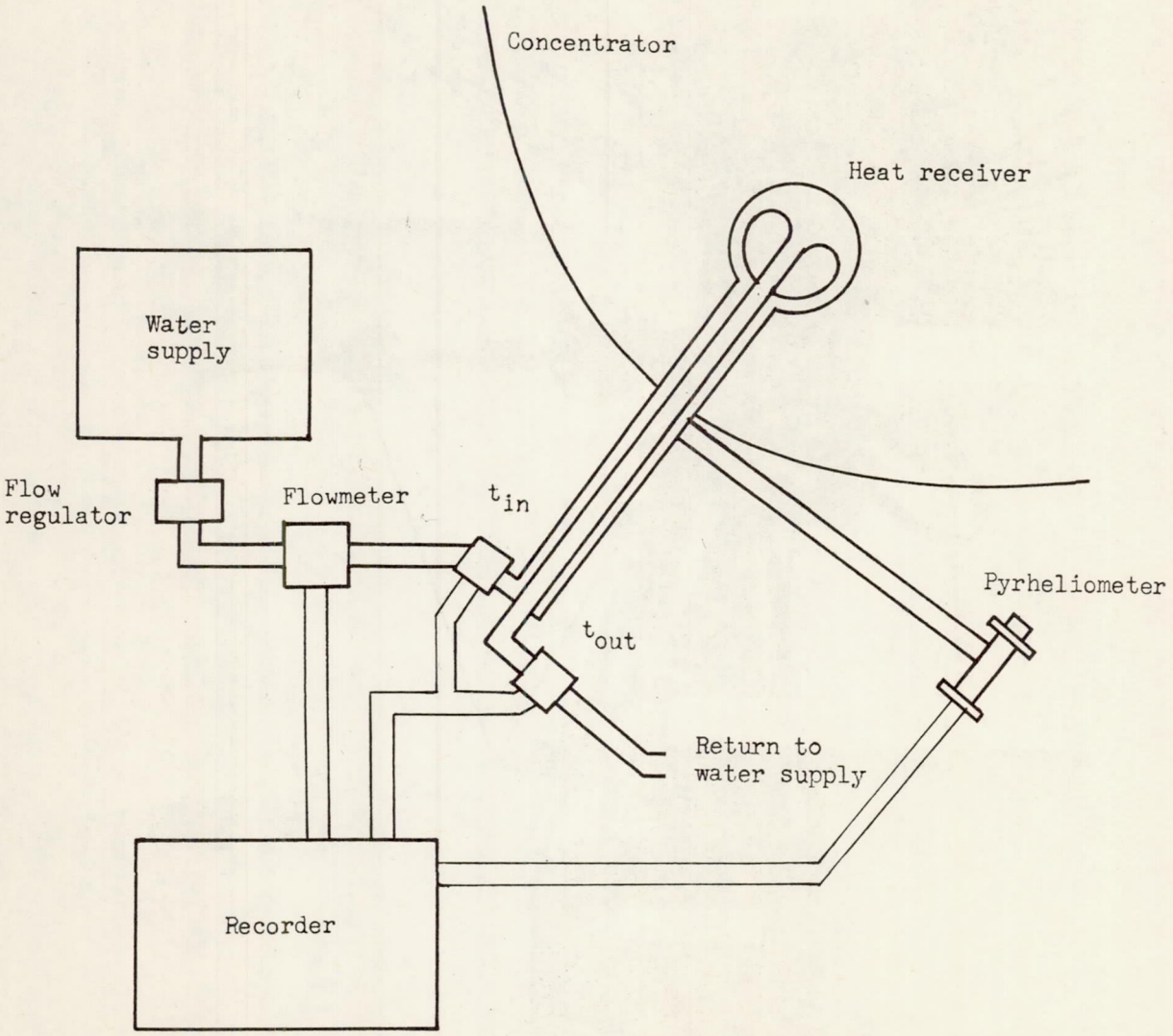

Figure 12.- Schematic drawing of solar concentrator test setup.

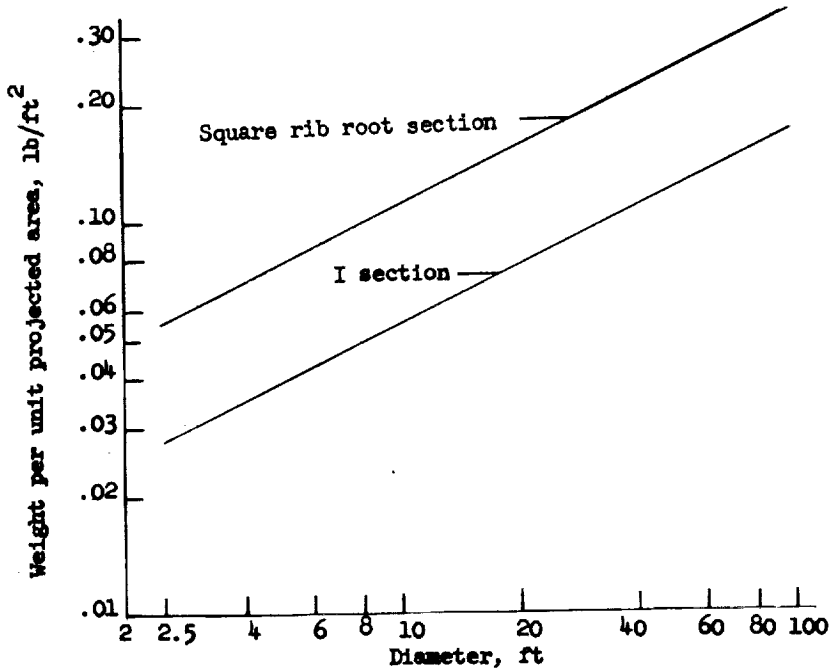

(a) Effect of rib shape on rib weight for aluminum rib.

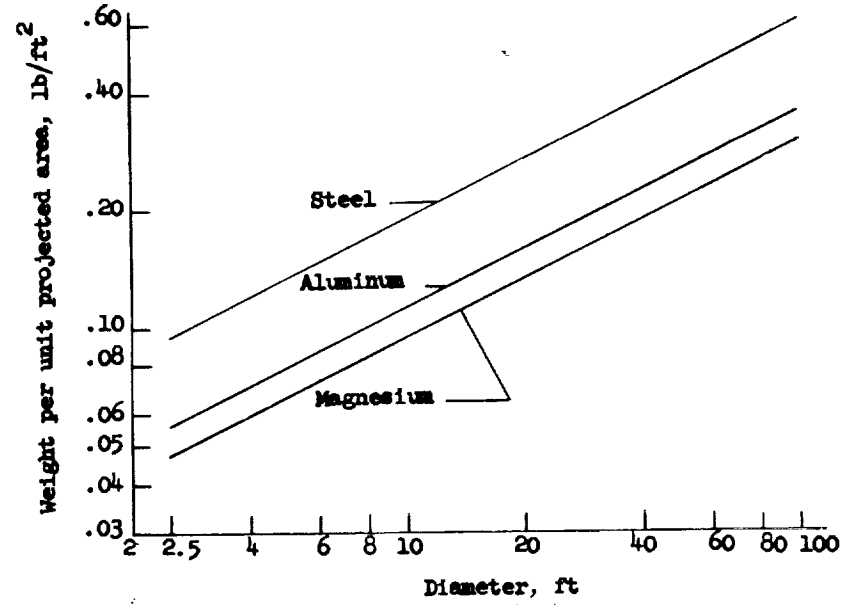

(b) Effect of material on rib weight for square rib root section.

Figure 13.- Effect of diameter on the rib weight per unit projected area.

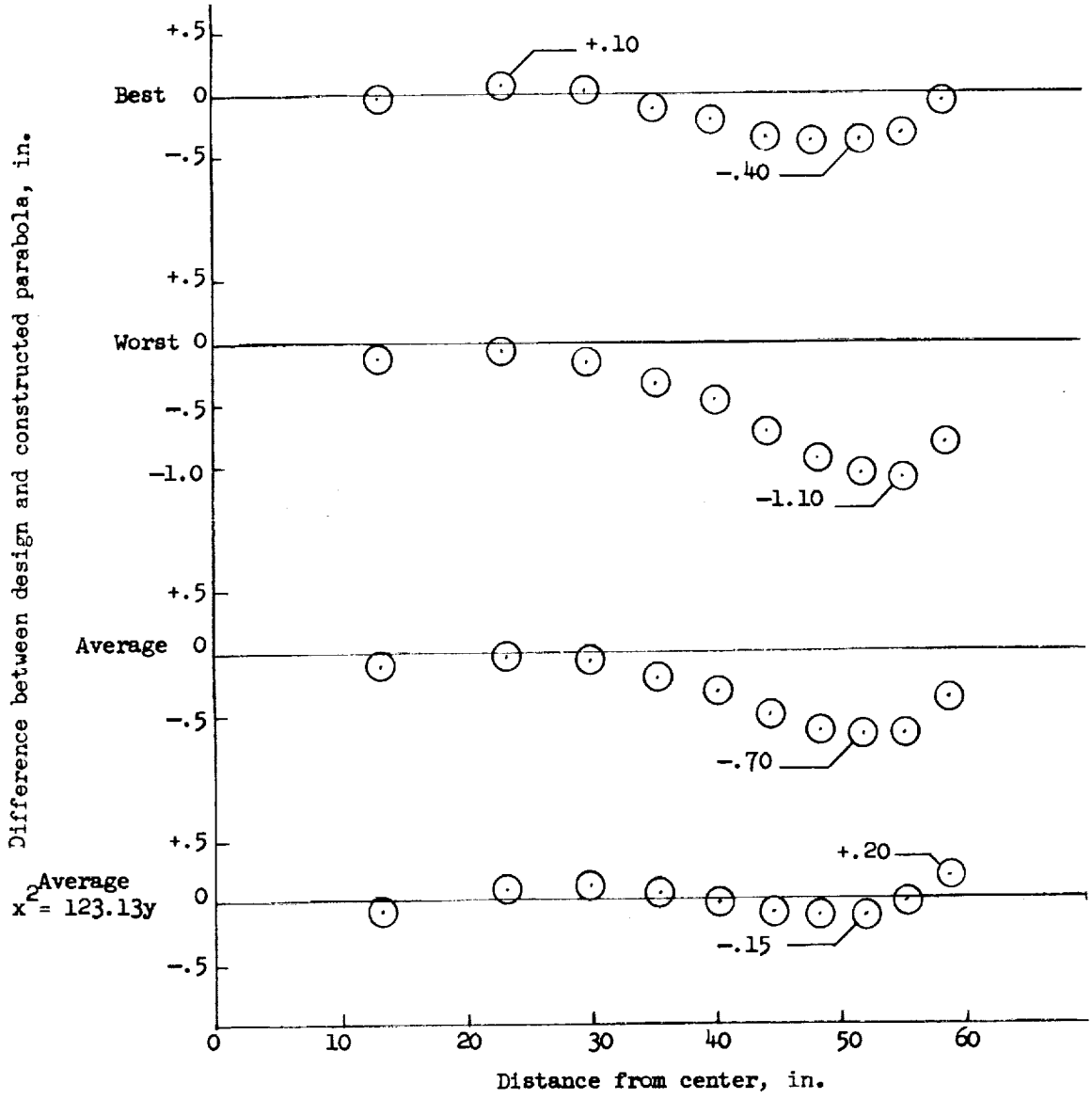

(a) Upright.

Figure 14.- Contour measurements of 10-foot-diameter concentrator ribs.

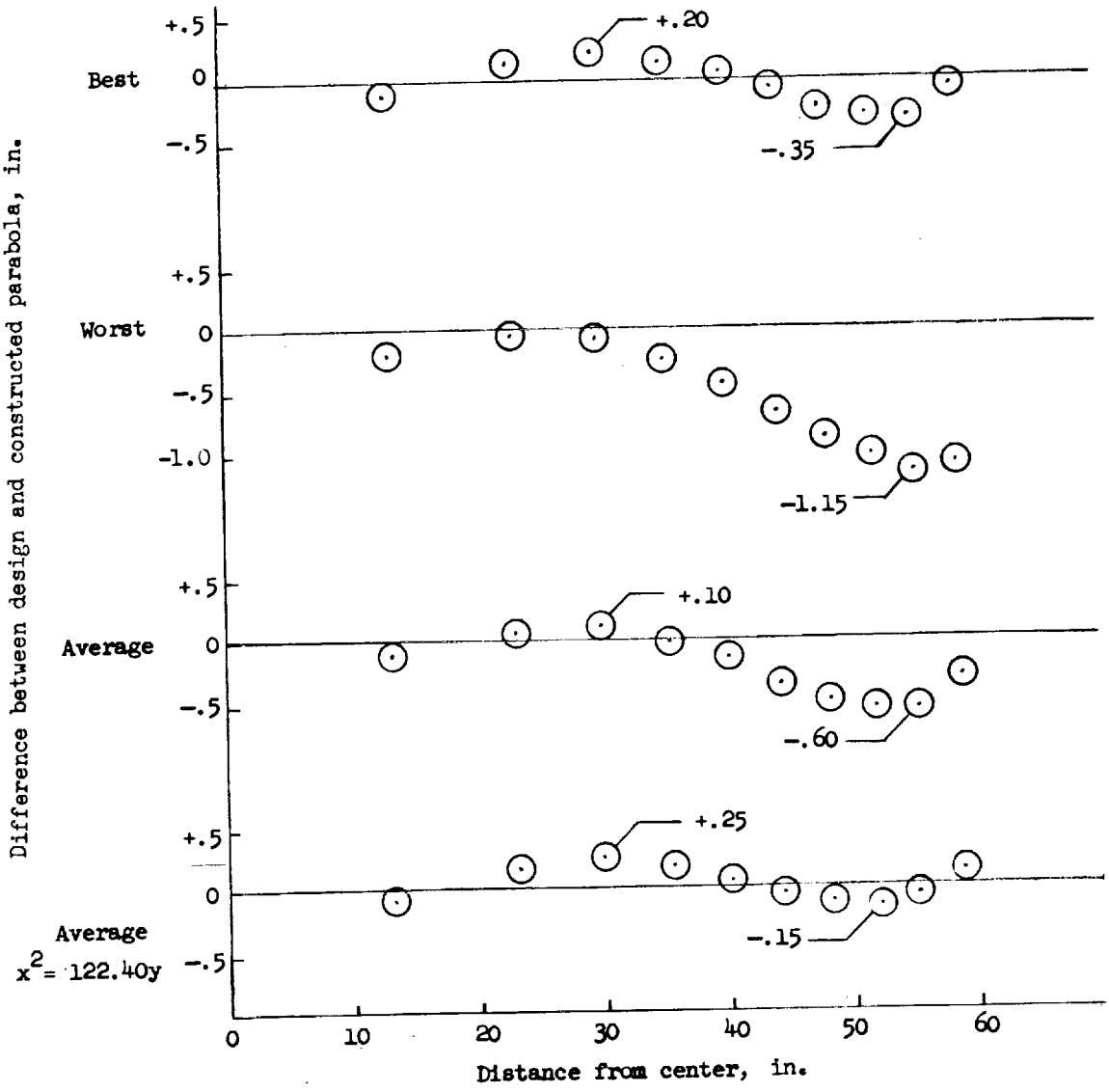

(b) Inverted.

Figure 14.- Continued.

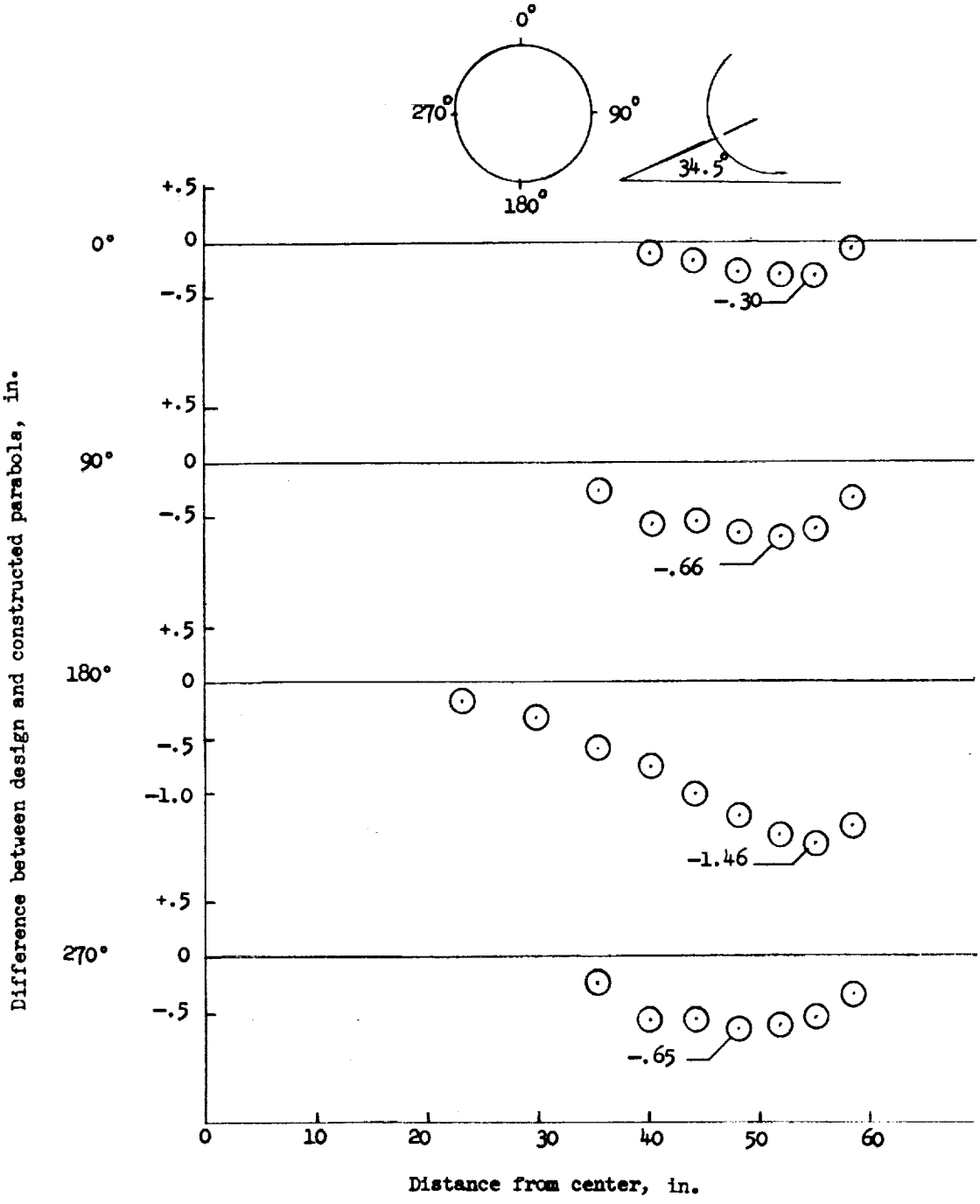

(c) Tilted at 34.5°.

Figure 14.- Concluded.

L-1371

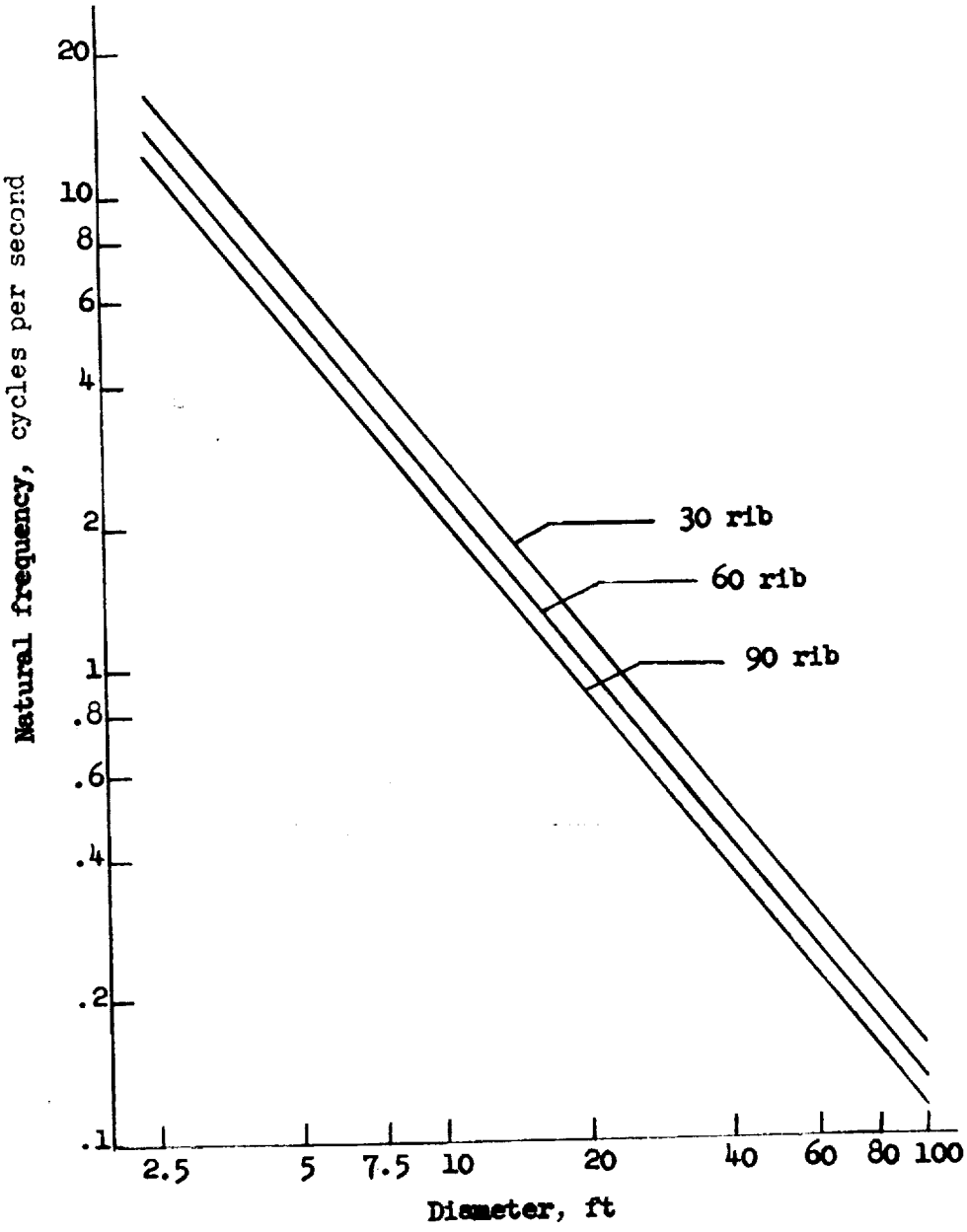

Figure 15.- Effect of concentrator diameter and number of ribs on rib natural frequency.

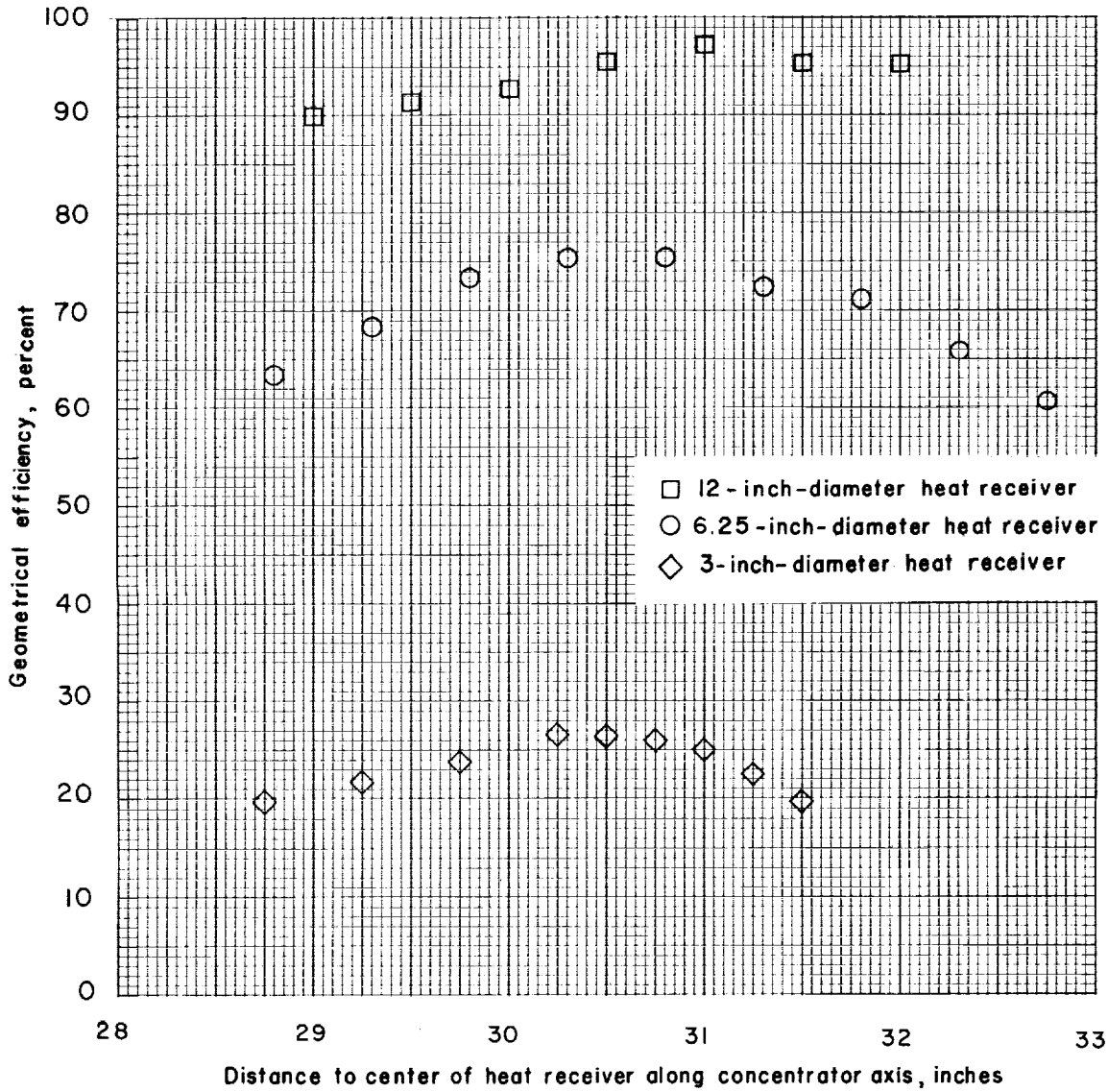

Figure 16.- Geometrical efficiency along the axis of the 10-foot-diameter concentrator with 1/2-mil surface.

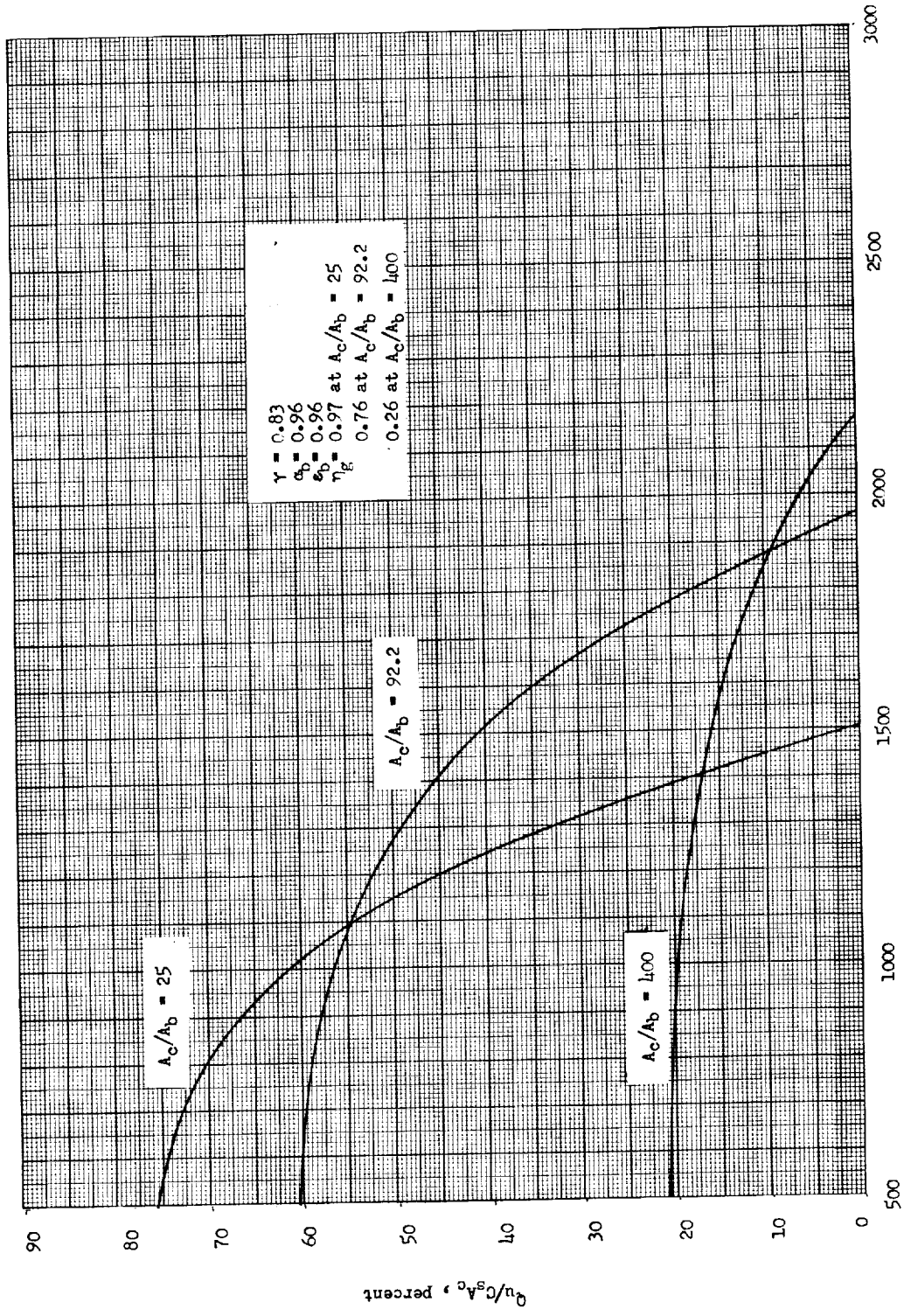

Figure 17.- Ratio of usable energy to available energy for various concentration ratios and receiver temperatures using experimental data.

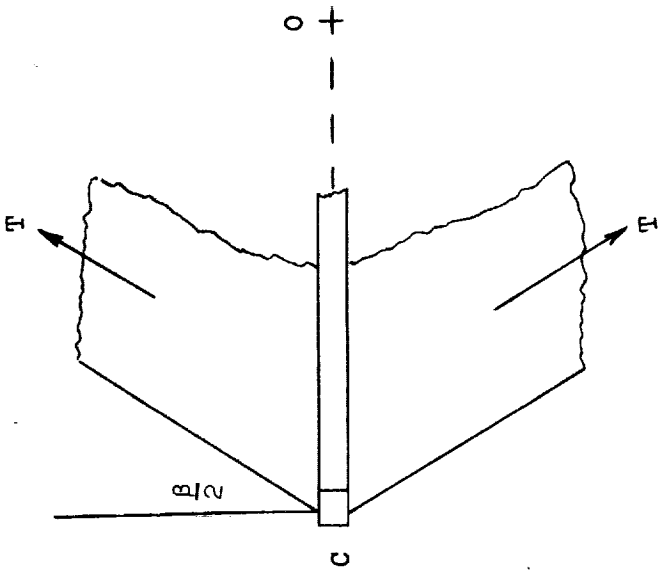

(b) Sketch of membrane tension acting on a rib.

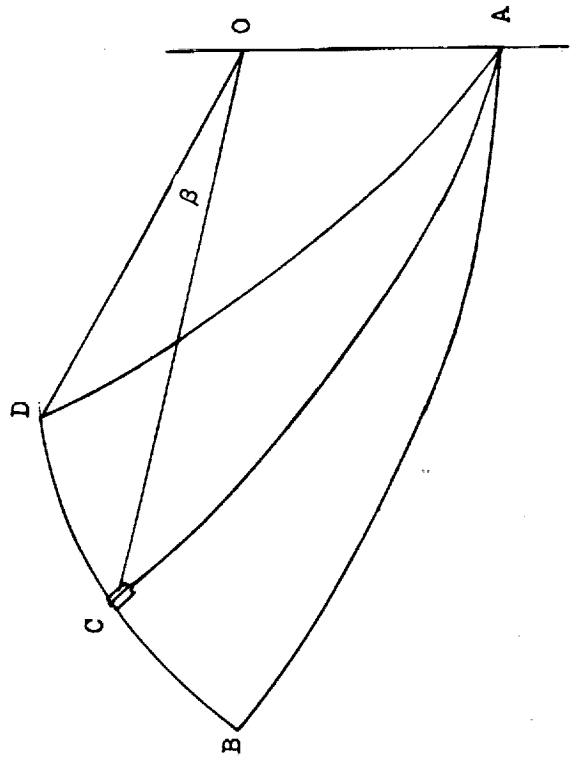

(a) Schematic diagram of a segment of the concentrator.

Figure 18.- View of concentrator ribs and membrane.

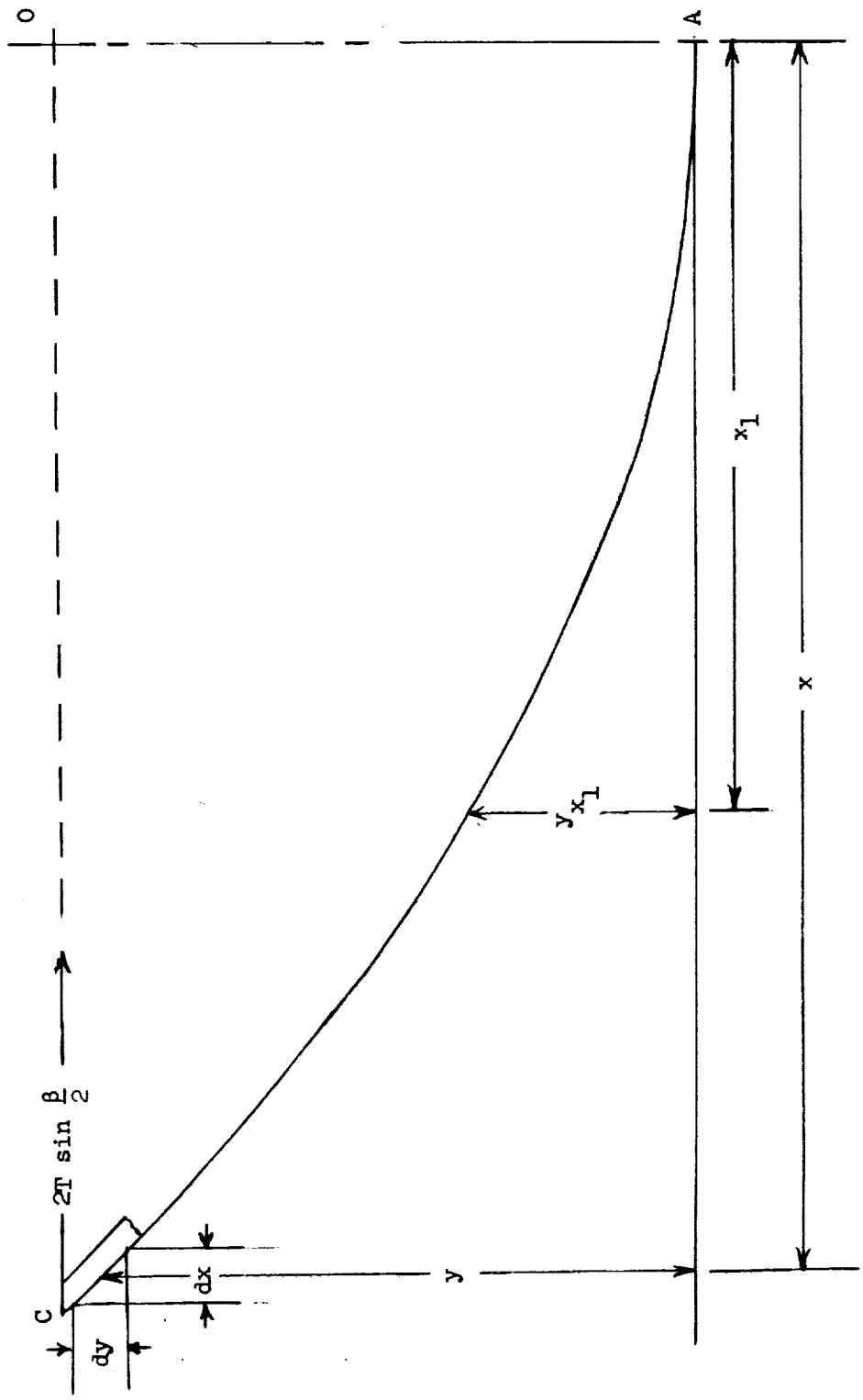

(c) Plane OAC.

Figure 18.- Concluded.